



저작자표시-비영리-변경금지 2.0 대한민국

이용자는 아래의 조건을 따르는 경우에 한하여 자유롭게

- 이 저작물을 복제, 배포, 전송, 전시, 공연 및 방송할 수 있습니다.

다음과 같은 조건을 따라야 합니다:



저작자표시. 귀하는 원저작자를 표시하여야 합니다.



비영리. 귀하는 이 저작물을 영리 목적으로 이용할 수 없습니다.



변경금지. 귀하는 이 저작물을 개작, 변형 또는 가공할 수 없습니다.

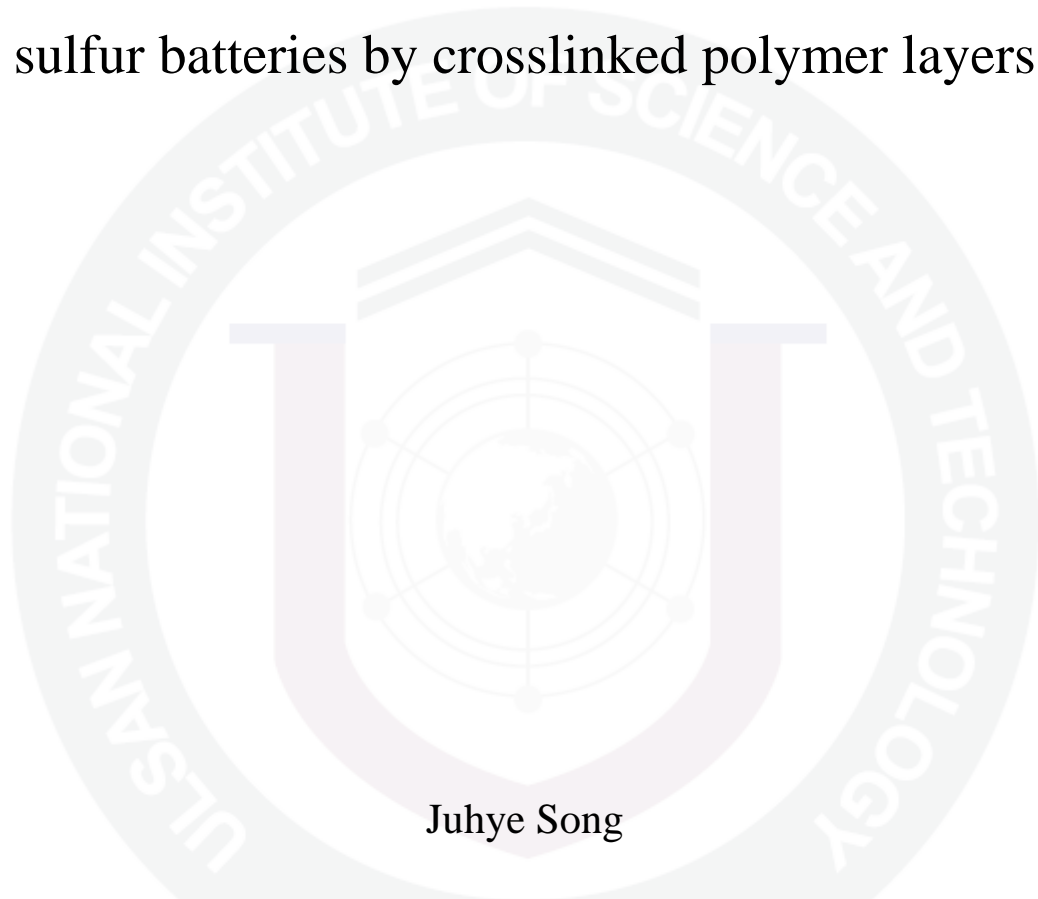
- 귀하는, 이 저작물의 재이용이나 배포의 경우, 이 저작물에 적용된 이용허락조건을 명확하게 나타내어야 합니다.
- 저작권자로부터 별도의 허가를 받으면 이러한 조건들은 적용되지 않습니다.

저작권법에 따른 이용자의 권리는 위의 내용에 의하여 영향을 받지 않습니다.

이것은 [이용허락규약\(Legal Code\)](#)을 이해하기 쉽게 요약한 것입니다.

[Disclaimer](#)

Improved electrochemical performance of lithium-sulfur batteries by crosslinked polymer layers



Juhye Song

Battery Science and Technology Program
Graduate School of UNIST

2014

Improved electrochemical performance of lithium-sulfur batteries by crosslinked polymer layers

Juhye Song

Battery Science and Technology Program
Graduate School of UNIST

Improved electrochemical performance of lithium-sulfur batteries by crosslinked polymer layers

A thesis

submitted to the Graduate School of UNIST

in partial fulfillment of the
requirements for the degree of
Master of Science

Juhye Song

01. 22. 2014

Approved by



Major Advisor

Nam-Soon Choi

Improved electrochemical performance of lithium-sulfur batteries by crosslinked polymer layers

Juhye Song

This certifies that the thesis of Juhye Song is approved.

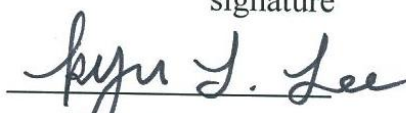
01.22. 2014 of submission

signature



Thesis supervisor: Nam-Soon Choi

signature



Kyu Tae Lee

signature



Sung You Hong

Abstract

Lithium sulfur (Li-S) battery is new generation system. Sulfur is widely known as a high theoretical capacity (1672 mAh g^{-1}) and high theoretical energy density (2600 Wh kg^{-1}). The attractive features of sulfur are low cost, abundant resources and nontoxic. Sulfur (S) is utilized as a cathode material and Li metal is an anode in Li-S cells. Since Li metal has high theoretical capacity of about 3860 mAh g^{-1} and the most electropositive (-3.04V versus standard hydrogen electrode), a high energy density can be achieved. During the discharge process, elemental sulfur (S_8) electrochemically reduces to soluble long-chain polysulfides and the resulting polysulfides can be dissolved into the electrolyte. Dissolved long-chain lithium polysulfide can diffuse to the Li anode and short-chain intermediate species (insoluble Li_2S_2 and Li_2S) may deposit on the anode, leading to the formation of unstable and non-uniform solid electrolyte interphase (SEI) layer. It can cause considerable capacity fading and safety concern related to the dendritic Li generated by non-uniform current distribution of the Li anode. These are important issues about thermal stability in all battery systems. In this study, we aim to understand thermal properties of sulfur cathodes and improve electrochemical performance of Li-S cells.

In chapter II, we investigate exothermic peaks for sulfur cathode according to different depth of discharge and fully charge step compared to delithiated lithium metal oxide cathode in a Li-ion battery by using the DSC technique. The exothermic peak of lithiated and delithiated sulfur cathode in the battery is considerably reduced at around $360 \text{ }^\circ\text{C}$. Also surface changes of the sulfur cathode were clearly demonstrated by ex-situ XPS technique during the different depth of discharge and fully charge processes. The thermal reaction between lithium metal and sulfur generated catastrophic exothermic heat in the presence of the ether-based electrolyte, but, the mixture of Li metal and lithium sulfide (Li_2S) showed greatly reduced exothermic peak.

In chapter III, we demonstrate the positive impact of the protective film on electrochemical properties of lithium metal anode in Li-S cells. Li metal, which is very reactive anode material, readily undergoes the reactions with polysulfides dissolved from the sulfur cathode. It is expected that the introduction of a protection layer based on the crosslinked gel polymer (semi-IPN structure) prevents unwanted reactions with polysulfide. Li-S cells without the protection layer show significant overcharge behavior during 10cycles, while the cell with protection layer effectually mitigates the overcharging.

Contents

CHAPTER I	1
1. Introduction	1
1.1. New generation battery system : Li-S battery.....	1
1.2. Mechanism of lithium sulfur battery	2
2. Improvements of sulfur battery system	8
2.1. Sulfur cathode	8
2.2. Lithium metal anode.....	8
3. Research objectives	10
CHAPTER II. Thermal reactions of lithiated and delithiated sulfur electrodes in lithium sulfur batteries	11
1. Introduction	11
1.1. Thermal stability of lithiated and delithiated sulfur cathode.....	11
1.2. Research objectives	12
2. Experimental	13
2.1. Lithium sulfur cell preparation and assembling.	13
2.2. Electrochemical cycling test	13
2.3. Preparation of samples for DSC measurement.....	13
2.4. Ex-situ X-ray photoelectron spectroscopy.....	14
2.5. FE-SEM	14
3. Results and discussion	15
3.1. Morphology of sulfur cathodes and Li metal anode surface along different depth of discharge and charge	15
3.2. Surface analysis of sulfur cathode at different depth of discharge and charge	18
3.3. Thermal stability characteristics of sulfur cathode	20
4. Conclusions	25
CHAPTER III. The introduction of crosslinked gel polymer structure on a lithium anode for improving electrochemical performance of lithium sulfur batteries.....	26
1. Introduction	26
1.1. Li metal as an anode	26
1.2. Problems of lithium metal electrode	26
1.3. The role of the protection layer on lithium anode	27

1.4. Research objectives	29
2. Experimental	30
2.1. Preparation of semi-IPN gel-polymer matrix	30
2.2. Lithium sulfur cell preparation and assembling.....	30
2.3 Electrochemical cycling test.....	30
2.4. Electrochemical analysis	31
2.4.1. FE-SEM	31
2.4.2. EIS (Electrochemical Impedance spectroscopy) and ATR-FTIR.....	31
2.4.3. Refrigerated Bath Circulation.....	31
3. Results and discussion	34
3.1. Effect of fluoroethylene carbonate (FEC) based electrolyte on interfacial lithium anode..	34
3.2. ATR-FTIR analysis of crosslinked polymer.....	34
3.3. Electrochemical properties in accordance with the crosslinkers in protection layer.	39
3.4. The characteristic of c-rate cycling according to protection layer	40
4. Conclusions	47
 References	 48

LIST OF FIGURES

Figure 1. Various new generation battery system required for future.

Figure 2. A schematic of typical charge and discharge work of lithium ion batteries.

Figure 3. A schematic illustration of (a) various intermediate species in voltage profile (top), and (b) multi-step electrochemical process for lithium/sulfur batteries (bottom).

Figure 4. The SEM images of (a) fresh Li metal surface before cycle (on the left) and of (b) dendritic lithium layer on Li surface after cycles (on right side).

Figure 5. (a) First discharge and charge profiles of a Li-S cell between 1.5 and 2.8 V vs. Li/Li⁺ at a current density of 83.6 mA g⁻¹ (C/20). (b) Schematic drawing for a multistep phase transformation process of cyclo-S₈ to form various intermediate species (Li₂S_n, n=1~8).

Figure 6. Photo of electrolyte solutions on the Li anodes at A, B, C, and D points (top). SEM images of the non-cycled sulfur cathode and the sulfur cathodes at A, B, C, and D points (middle). SEM images of the non-cycled Li anode and the Li anodes at A, B, C, and D points (bottom). All points are represented in Fig. 5(a).

Figure 7. C1s, F1s, S2p XPS spectra of sulfur cathodes (a) discharged up to 2.3V, (b) discharged up to 2.02V, (c) fully discharged up to 1.5V, (d) fully charged up to 2.8V.

Figure 8. DSC heating curves of (a) sulfur cathode discharged to 2.3V, (b) sulfur cathode discharged to 2.02V, (c) sulfur cathode fully discharged to 1.5V, (d) sulfur cathode fully charged to 2.8V. All cathode samples for DSC measurements contain the electrolyte solution (1.3M LiTFSI in TEGDME). (e) Schematic for the thermal reactions of lithiated and delithiated sulfur cathodes in presence of TEGDME/1.3M LiTFSI. OLO represents over-lithiated layered oxides (Li_xMn_yCo_zNi_aO₂ cathode).

Figure 9. DSC heating curves of (a) Li₂S + Li metal with an electrolyte, (b) Li metal with an electrolyte, (c) Li₂S with an electrolyte, (d) S + Li metal with an electrolyte, (e) S with an electrolyte, (f) 1.3M LiTFSI in TEGDME electrolyte. (g) Comparison between S + Li metal with an electrolyte showing the exothermic peak at 176 °C and Li₂S + Li metal with an electrolyte.

Figure 10. DSC heating curves of (a) Li₂S powder, (b) Sulfur powder, (c) Li₂S + Li metal, (d) S + Li metal in absence of an electrolyte.

Figure 11. The graph of potential vs capacity of various cathode and anode materials.

Figure 12. The non-uniform current distribution and high reactivity for lithium metal anode.

Figure 13. Schematic of internal lithium sulfur system of (a) non-protected lithium and of (b) protected lithium anode.

Figure 14. Galvanostatic cycling of Li symmetric cells with FEC- and TEGDME-based electrolytes.

Figure 15. (a) Voltage profile of precycle at a rate of C/20. (b) EIS spectra of cells with various amounts of FEC-based electrolyte in a protection layer. (c) Cycling performance of Li-S cells with

various amounts of FEC- based electrolyte in protection layer at a rate of C/10 .

Figure 16. SEM images of (a) fresh lithium metal surface, (b) crosslinked protective layer and (c) image of cross-section about thickness of protective layer.

Figure 17. ATR-FTIR spectra for (a) BDDA, (b) TMPETA 428 crosslinkers. Spectra of crosslinked protection layer in present of (c) BDDA and (d) TMPETA 428 crosslinkers (after UV-curing).

Figure 18. Cycling performance according to type of crosslinkers and in the presence of protection layer in lithium anode. (a) Voltage vs specific capacity profile, (b) charge capacity, (c) discharge capacity, (d) coulombic efficiency during 100cycles at a C/10 rate at 30 °C.

Figure 19. SEM images of lithium surface morphology. SEM images of (e) ~ (j) are lithium surface removed protection layer according to cycles.

Figure 20. SEM images of lithium surface morphology. SEM images of (a) ~ (g) are morphology of protection layer on lithium surface according to cycles.

Figure 21. Change the color of the protection layer surface according to cycles. After (a) precycle, (b) 5cycles, (c) 10cycles, (d) 30cycles.

Figure 22. Change the color of the separator surface with the cycle number. (a) precycle, (b) 5cycles, (c) 10cycles, (d) 30cycles.

Figure 23. Comparison of the elemental S mapping images of (a) exposed lithium surface and of (b) protection layer surface after 10cycles.

Figure 24. C-rate characteristics according to the kind of crosslinkers. (a) Discharge capacity, (b) coulombic efficiency.

Figure 25. Comparison of the ionic conductivity of the crosslinked gel polymer according to the kind of the crosslinkers.

LIST OF TABLES

Table 1. Characteristics of several types of rechargeable lithium batteries..

Table 2. Chemical structure of linear polymer, crosslinkers, and photoinitiator for protection layer,

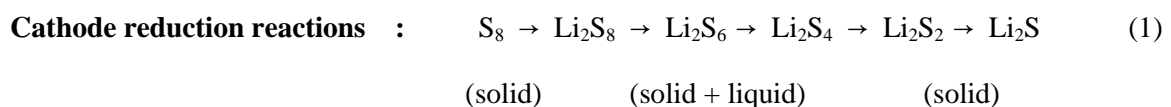
Table 3. Composition of protection layer.

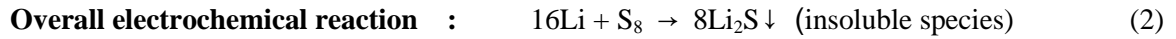
CHAPTER I

1. Introduction

1.1 New generation battery system : Li-S battery

According to meet the stringent requirements of emerging market, the rapid demanding of power sources for portable devices and electric vehicles calls for the advanced batteries with high specific energy density likewise long life and cost effective. That's why rechargeable lithium ion batteries already being commercialized are being developed because of their specific energies in the range 100-150 Wh kg⁻¹ as shown in Table 1 and Fig. 1.^{1,2} Lithium sulfur batteries were introduced in the 1960s.^{3,4} Lithium-sulfur redox behavior, one of the most promising candidates, has high theoretical capacity of elemental sulfur as cathode electrode and lithium metal as an anode material, which corresponds to 1672 and 3860 mAh g⁻¹ respectively and also has high theoretical energy density (2600 Wh kg⁻¹).^{1,2} It is about 3~5 times higher than any commercialize lithium ion batteries, which is widely used in our society.⁵ The average operation voltage is 2.15V that is suitable for low voltage electronic devices.⁶ In addition, lithium sulfur batteries have many attractive features such as natural abundance, low cost and non-toxic. Also this system is allowed to operate at low-temperature up to -60 °C.^{7,8,9} General LIB (lithium ion battery) operates by oxidation of Li ion from metal oxide cathode (LCO, NCM, LMO₂, etc.) to anode (graphene structure) on charge step through liquid electrolyte. Moved lithium ions are inserted between layers of the graphite. In discharge process, inserted lithium ions are moved back to the cathode as shown in Fig. 2.² This whole reaction can be called intercalation and de-intercalation cycle.¹⁰ Contrary, lithium sulfur cells operate by reduction of Li ion from anode (purity Li metal foil) to cathode (elemental cyclo-S₈, starting material) on discharge step. It usually occurs two plateaus in discharge voltage profile. At the first plateau (~2.3 V vs. Li⁺/Li), sulfur is reduced from S₈ to S₄²⁻, during which various electrolyte-soluble long polysulfides (Li₂S_n, n = 4-8) form (Eq. 1). The second plateau (~1.95 V vs. Li⁺/Li) corresponds to the transformation from Li₂S₄ to insoluble Li₂S₂ and finally Li₂S (Fig. 3(a) and Eq. 2).⁸ The reaction is as follow :¹¹





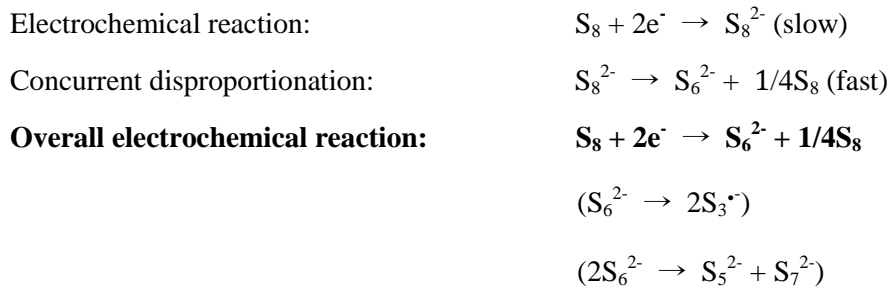
In charge process, the soluble short-chain lithium polysulfides will diffuse back to the cathode partially and then be reoxidized to long-chain lithium polysulfides. This so-called internal shuttle mechanism as shown in Fig. 3(b).^{12,13,14,15}

1.2 Mechanism of lithium sulfur battery.

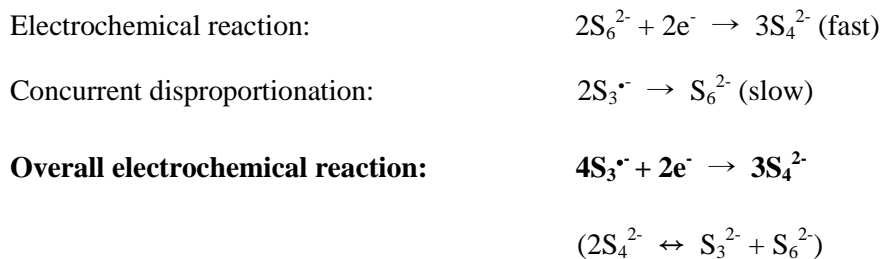
It is very difficult to define the exact charge-discharge mechanism of lithium sulfur system and still controversial. Some researchers discuss many complex intermediate-lithium polysulfides species such as S_8^{2-} , S_6^{2-} , S_4^{2-} , S_3^{2-} , $\text{S}_3^{\cdot-}$, S_2^{2-} respectively.^{16,17,18,19} Recently, *Fannie Alloin et al.* reported a possible sulfur reduction mechanism of three multi-steps. They proved intermediate sulfur species in reduction cycle by using UV and HPLC data.²⁰ The equations are as follow :

EQUATIONS

- **1st step (~2.4V vs. Li⁺/Li)**



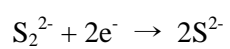
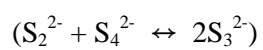
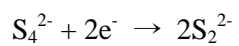
- **2nd step (~2.1V vs. Li⁺/Li)**



- **3rd step (~2V vs. Li⁺/Li)**



Or



Overall electrochemical reaction: $S_4^{2-} + 6e^- \rightarrow 4S^{2-}$

$S_3^{\cdot -}$ radical is produced due to disproportionation reaction. All intermediate species are continuously formed.

Table 1.Characteristics of several types of rechargeable lithium batteries.¹

Li battery couple	Theoretical specific energy (Wh/kg)	Practical specific energy (Wh/kg total cell)	Theoretical specific capacity (mAh/g active material)	Practical specific capacity (mAh/g total cell)
Li/Li _x Mn ₂ O ₄	428	120	285 (x=2)	100-120
LiC ₆ /Li _x CoO ₂	570	180	273 (x=1)	136
Li/Li _x V ₆ O ₁₃	890	150	412 (x=8)	309
Li/Li _x TiS ₂	480	125	225 (x=1)	58
Li/S	2600	-	1672	> 200 ^a

^a Based on positive electrode only, with 50% sulfur. Capacity data is for cycle regimen yielding the longest cycle.

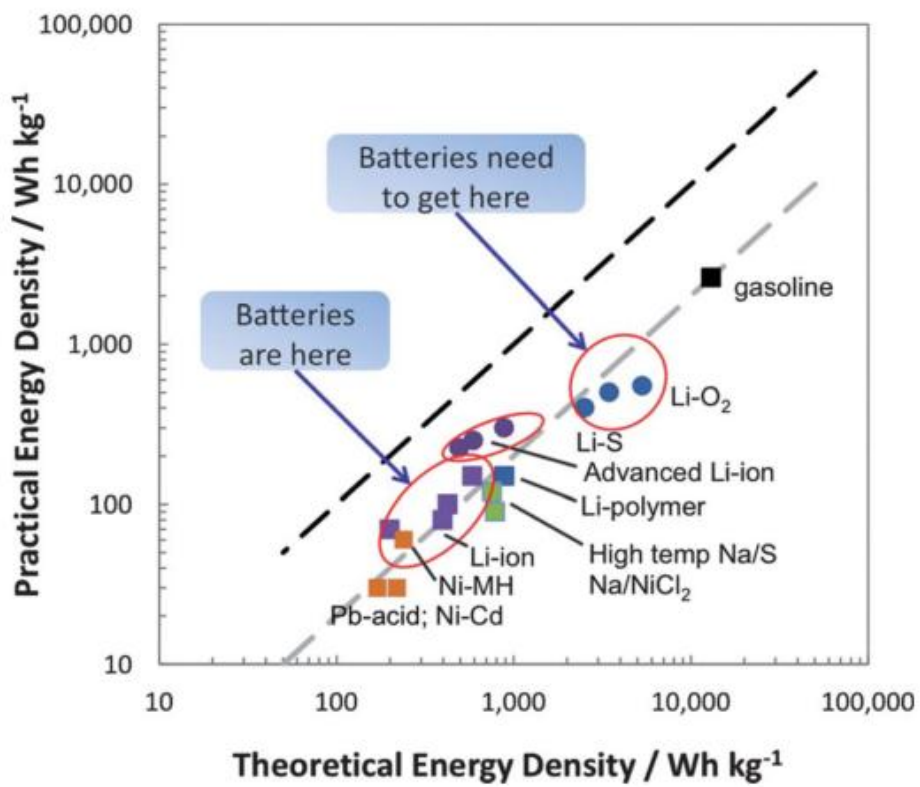


Figure 1. Various new generation battery system required for future.²

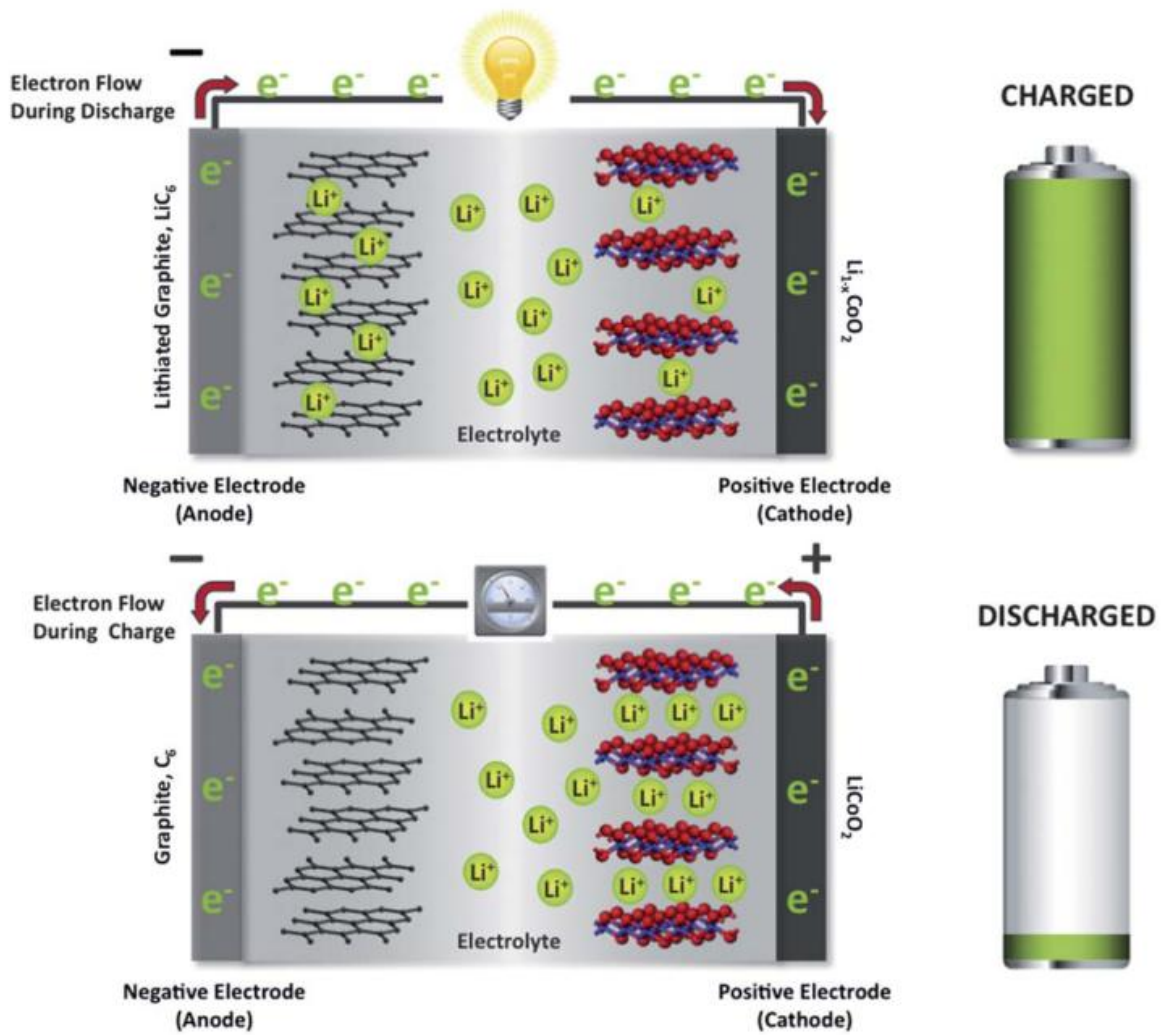


Figure 2. A schematic of typical charge and discharge work of lithium ion batteries.²

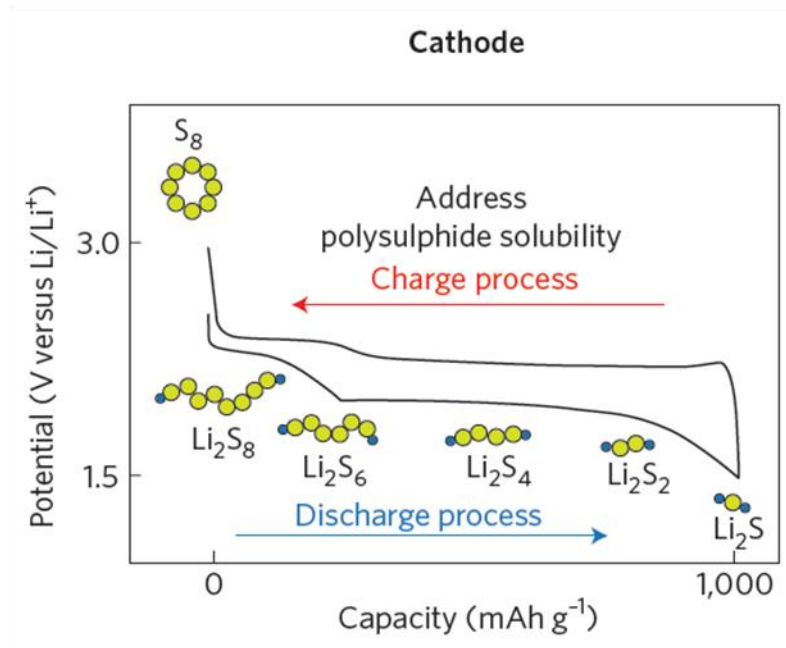
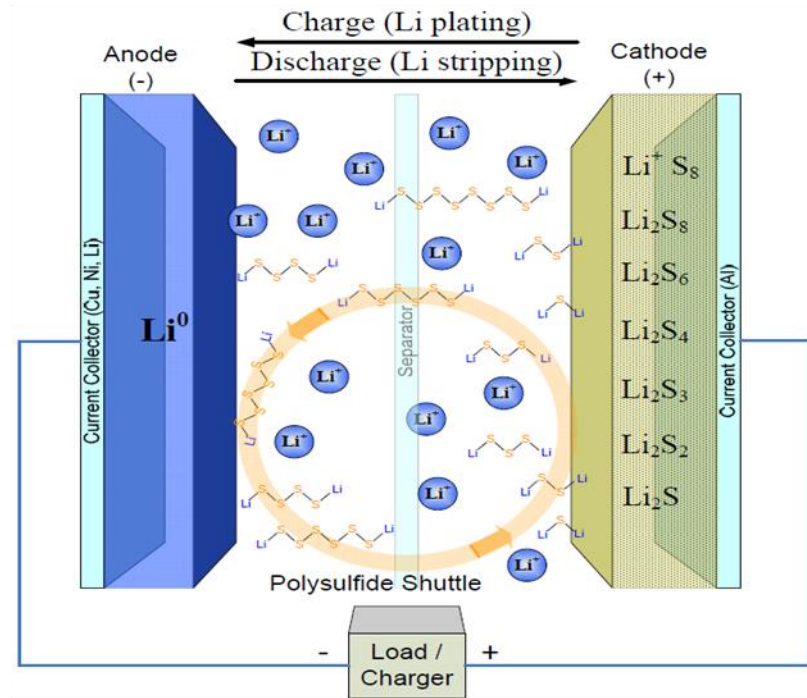
(a)**(b)**

Figure 3. A schematic illustration of (a) various intermediate species in voltage profile (top),⁸ and (b) multi-step electrochemical process for lithium/sulfur batteries (bottom).^{Sion power}

2. Improvements of sulfur battery system

2.1. Sulfur cathode

In spite of many attractive features of lithium sulfur batteries, there are still many problems to be overcome for practical applications. Elemental sulfur (S_8) cannot be used alone as cathode material. The electrical conductivity of sulfur is too low as 5×10^{-30} S/cm at 25°C .²¹ Such a low conductivity causes poor electrochemical contact of the sulfur and leads to low utilization of active materials in the cathode.⁶ The sulfur, including porous carbon and conducting agent is significantly improved electrical conductivity of sulfur.^{5,12,22} A wide variety of conducting agents can transport electrons between current collector and active materials. S_8 and soluble long chain lithium polysulfides (Li_2S_n , $n = 4-8$) can dissolve in ether-based electrolyte easily. Dissolved intermediate-lithium polysulfides can diffuse to the lithium anode and form insoluble Li_2S_2 or Li_2S . And then this can deposit on the anode and elsewhere.^{8,23,24} This acts as an insulator, part of insulating reaction products cover the sulfur particles and prevent further electrochemical reaction.²⁵ In order to improve the disadvantages of cathode property, many efforts have been made to improve the performance of sulfur by using various conducting substrates and new carbon/sulfur composite structure to prevent dissolution of soluble polysulfides in electrolyte.

2.2. Lithium metal anode

Lithium as an anode electrode is very reactive material. During charge and discharge cycling, dendrites on the lithium surface are constantly created and forms unstable SEI layer as shown in Figs. 4(a) and 4(b). It gives rise to thermal runaway and leads to an explosion hazard during operation, resulted in poor cycle performance and low active material utilization due to the insoluble Li_2S_2 or Li_2S . The introduction of unique additive like a LiNO_3 and protection layer can effectively protect on the lithium surface.^{6,26,27,28,29,30} These can control morphology of SEI layer, suppressing dendrite formation and possible controlling decomposition products. Also passivation layer is role of blocking the reaction of lithium metal with polysulfides (Li_2S_n).

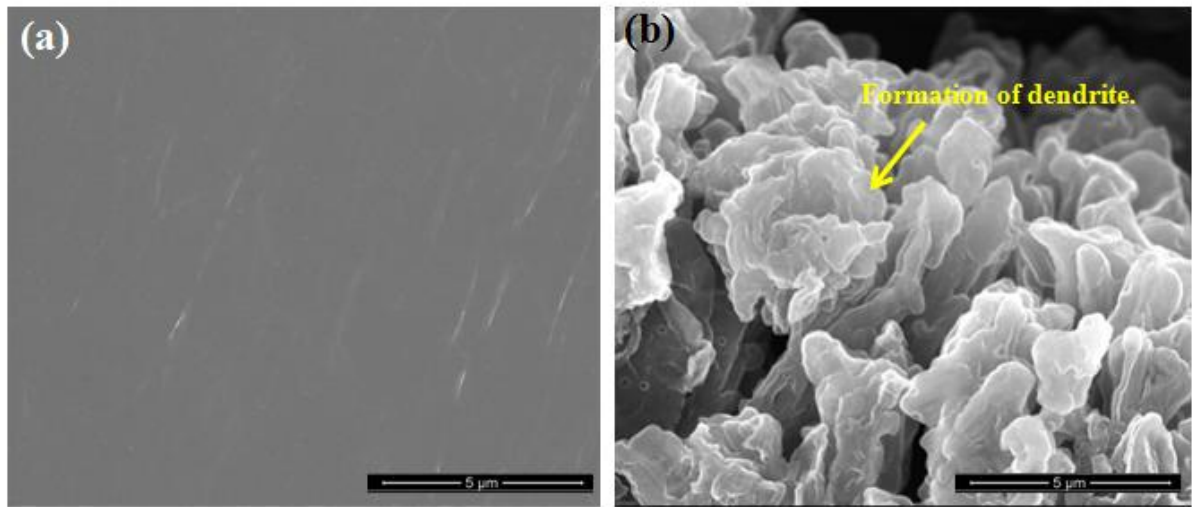


Figure 4. The SEM images of (a) fresh Li metal surface before cycle (on the left) and of (b) dendritic lithium layer on Li surface after cycles (on right side).

3. Research objectives

This dissertation is divided into two kinds of subjects. In chapter **II**, it can be explained about thermal stability of sulfur cathode with 1.3M $\text{LiN}(\text{SO}_2\text{CF}_3)_2$ in tetra(ethylene glycol) dimethyl ether (TEGDME) according to different of depth as well as fully discharge and fully charge process during first cycle by using differential scanning calorimetry (DSC). In addition, it is indicated a detailed investigated of the electrochemical reaction products on the sulfur cathode by means of ex-situ X-ray photoelectron spectroscopy (XPS). Through this experiment, it can be compared the thermal reactions of a lithiated and delithiated sulfur and oxide based cathode material with 1.3M LiPF_6 in carbonated based co-exist electrolytes.

In chapter **III**, here is the most important subject that protection and enhance the lithium surface. It can be explained about stability of lithium interfacial between lithium metal and liquide electrolytes including soluble long chain lithium polysulfides. Though galvanostatic cycling performance for Li-symmetric cell, it shown that FEC-based electrolyte in crosslinked gel polymer (semi-IPN structure) is stable on the surface of lithium anode. By introducing the crosslinked gel polymer on lithium surface, it can be reduced the reaction between lithium and lithium polysulfides, which is diffused from cathode electrode. Therefore, severe capacity fading and overcharge process can be improved during long cycling. One more important study, various types of crosslinkers have a unique cycling behavior, depending on density of cross-linking. This part also used 1.3M $\text{LiN}(\text{SO}_2\text{CF}_3)_2$ in tetra(ethylene glycol) dimethyl ether (TEGDME) as bulk electrolyte.

CHAPTER II

Thermal reactions of lithiated and delithiated sulfur electrodes in lithium sulfur batteries

1. Introduction

1.1. Thermal stability of lithiated and delithiated sulfur cathode

Elemental sulfur has been extensively investigated as a promising candidate for cathode materials, largely on the basis of its high theoretical specific capacity of 1672 mA h g^{-1} , abundance, low cost, and environmentally benign characteristics.^{24,31,32,33} However, achieving long-term cycle life of lithium-sulfur (Li-S) batteries is formidable because of the electrical insulating nature of elemental sulfur and the formation of long chain polysulfide intermediates (Li_2S_n , $n = 4\sim 8$), which are soluble in the electrolyte.^{15,23} Interestingly, non-lithiated sulfur cathode materials provide improved safety because they cannot be overcharged, unlike lithium metal oxides. LiCoO_2 , which has been the main Li-ion battery cathode material, suffers from safety issues. LiCoO_2 charged up to 4.5V vs. Li/Li^+ , showed an extremely sharp exothermic peak at around 212°C and large exothermic heat of 2785 J g^{-1} .³⁴ Thermal runaway is caused by thermal reactions between the electrolyte and lithiated anodes or between the electrolyte and delithiated cathode in the battery. To the best of our knowledge, there have been no studies on the thermal reactions between various polysulfide intermediates formed during cycling of Li-S batteries and a liquid electrolyte. During the lithiation process, sulfur is electrochemically reduced to Li_2S_n ($n = 4\sim 8$) at the upper potential plateau region ($\sim 2.3 \text{ V vs. Li/Li}^+$); this Li_2S_4 is further reduced to insoluble Li_2S_2 and finally Li_2S at the lower plateau region ($\sim 2.1 \text{ V vs. Li/Li}^+$).^{35,36}

1.2. Research objectives

In this study, we attempt to broaden the understanding of the thermal reactions of long- and short-chain polysulfide intermediates formed by electrochemical reduction of the sulfur cathode in Li-S batteries. The thermal reactions of a lithiated and delithiated sulfur electrode with 1.3M $\text{LiN}(\text{SO}_2\text{CF}_3)_2$ in tetra(ethylene glycol) dimethyl ether (TEGDME) are investigated by differential scanning calorimetry (DSC). In addition, we have conducted a detailed investigation of the electrochemical reaction products on the sulfur cathode by means of ex-situ X-ray photoelectron spectroscopy (XPS).

2. Experimental

2.1. Lithium sulfur cell preparation and assembling

For the electrochemical tests, a mixture of 70 wt% elemental sulfur (100 mesh, Aldrich) and 20 wt% super P (as a carbon additive for conductivity enhancement, Timcal Inc.) was ball-milled, and then a 10 wt% poly(vinylidene fluoride) (PVDF) ($M_w = 534,000$, Aldrich) binder in anhydrous *N*-methyl-2-pyrrolidinone (NMP, Aldrich) was added to the mixture. After mixing the cathode slurry by using thinky mixer during 10min, it was cast on a piece of aluminum foil (20 μm) and then dried in a convection oven at 90 $^{\circ}\text{C}$ for 1 h. The thickness of all cathode films was about 28 μm and the sulfur loading was 0.7 mg cm^{-2} . As the count electrode, fresh Li metal foil (700 μm) used on the copper foil current correcter. Cell assembly was performed in glove box with 1.3M lithium bis(trifluoromethane sulfonyl)imide (LiTFSI) in tetra(ethylene glycol) dimethyl ether (TEGDME) (received from Soulbrain Co. Ltd.).

2.2. Electrochemical cycling test

Galvanostatic discharge and charge cycling (WonATech WBCS 3000 battery measurement system) was performed in a potential window from 1.5 to 2.8 V versus Li/Li⁺ with a two-electrode 2032 coin-type cell. The sulfur cathode electrode functioned as the working electrode and the Li metal foil as the counter electrode. The first lithium insertion and extraction capacities were measured at a current density of 83.6 mA g^{-1} (C/20 rate) at 30 $^{\circ}\text{C}$.

2.3. Preparation of samples for DSC measurement

To measure the thermal properties of cycled sulfur cathodes with electrolytes, coin full-cells at various discharged and charged states were carefully opened in a dry room. The retrieved electrodes were transferred into a hermetic stainless steel pan (Perkin Elmer) without a rinsing process. Thermal analyses of lithiated and delithiated sulfur cathodes and electrolytes were conducted by using a differential scanning calorimetry technique (DSC, Mettler Toledo). Each sample was scanned at a heating rate of 5 $^{\circ}\text{C min}^{-1}$ within an appropriated temperature range under a nitrogen atmosphere. The amount of entrapped electrolyte was 50 wt% based on the sulfur and Li₂S powder.

2.4. Ex-situ X-ray photoelectron spectroscopy

The cells were carefully opened in a glove box to retrieve their electrodes. The electrodes were then rinsed in 1,3-dioxolane to remove the residual LiTFSI-based electrolyte, and the resulting materials were dried. Ex-situ X-ray photoelectron spectroscopy (XPS, Thermo Scientific K-Alpha system) measurements for dried electrodes were performed with Al K α ($h\nu=1486.6$ eV) radiation under an ultrahigh vacuum. XPS spectra were taken using a 0.10 eV step and 50 eV pass energy. Samples were prepared in a glove box and sealed with an aluminum pouch film under a vacuum before use. The samples were then rapidly transferred into the chamber of the XPS instrument to minimize any possible contamination. All XPS spectra were energy calibrated by the hydrocarbon peak at a binding energy of 284.8 eV.

2.5. FE-SEM

The surface morphology of the pristine or cycled sulfur cathodes along discharge and charge depth and Li metal anodes was observed by means of a field emission scanning electron microscope (FE-SEM; JEOL JSM-6700F). During the acquisition of the SEM image, an energy dispersive spectrometer (EDS) was also used to determine the kind of chemical components in the region under investigation. Sulfur cathodes and Li metal anodes retrieved from cells were put on a SEM holder in a glove box and the prepared samples were sealed with an aluminum pouch film under a vacuum. The samples were transferred from an aluminum pouch bag into a vacuum chamber for the SEM/EDX observation with exposure to atmosphere for 3 sec.

3. Results and discussion

3.1. Morphology of sulfur cathodes and Li metal anode surface along different depth of discharge and charge

Fig. 5(a) shows the voltage profile of the first discharge and charge of a Li-S cell. Electrochemical reduction of cyclooctasulfur (cyclo-S₈) in a Li-S cell is a multistep phase transformation process that forms various intermediate species (Li₂S_n, n=1~8), as depicted in Fig. 5(b). When the cell was discharged to point A, there was a significant color change in the electrolyte solution, as presented in photo A of Fig. 6. The color change indicates that the cyclooctasulfur molecule, S₈, is electrochemically transformed to Li₂S_n (n=8). The surface morphology of the sulfur cathode discharged to point A was analogous with the noncycled cathode, showing a distribution of carbon black that is responsible for the electronic conduction. This is because the formed soluble polysulfide species were removed by the rinsing process for SEM observation. The SEM image of the Li anode surface reveals that non-uniform micropores were produced by Li stripping. At point B, the color of the electrolyte changed from dark orange to orange. This indicates the formation of different products by phase transformation. Li₂S₈ formed at the first discharging plateau is reduced to Li₂S₄ during the further discharge process. Indeed, the surface of the sulfur cathode discharged to point B was covered with partly insoluble polysulfide species, as shown in the SEM image of Fig. 6. The surface morphology of the Li anode at point B was similar with that at point A. After the cell was fully discharged to 1.5V, the color of the electrolyte became light green-yellow rather than colorless.³⁶ This indicates that a Li₂S₂ or Li₂S compound with an insulating nature may block electron transfer to the interior of the sulfur cathode material and prevent complete reduction of short-chain polysulfides to Li₂S₂ or Li₂S. Therefore, soluble lithium polysulfide intermediates, which are not transformed to Li₂S₂ or Li₂S, exist in the cathode at a fully discharge state. As clearly seen in the SEM image of Fig. 6 (point C), the sulfur cathode was mostly covered with a thick velvety layer composed of an insoluble phase (Li₂S₂ or Li₂S), unlike the sulfur cathode at point B. SEM images of Fig. 6 reveal that the fully charged sulfur cathode did not return to its original surface morphology and had a velvety insoluble layer (Li₂S₂ or Li₂S), which is apparently formed at a fully discharged state. This indicates that the Li₂S₂ or Li₂S solid phase precipitated on the cathode during discharging hinders the complete oxidation of polysulfide back to elemental sulfur and partly insoluble short-chain polysulfide coexists with elemental sulfur in the sulfur cathode at a fully charged state. At point D, the color of the electrolyte was more deeply orange compared to the color at point C. This indicates the existence of soluble long-chain polysulfide species in the electrolyte solution.

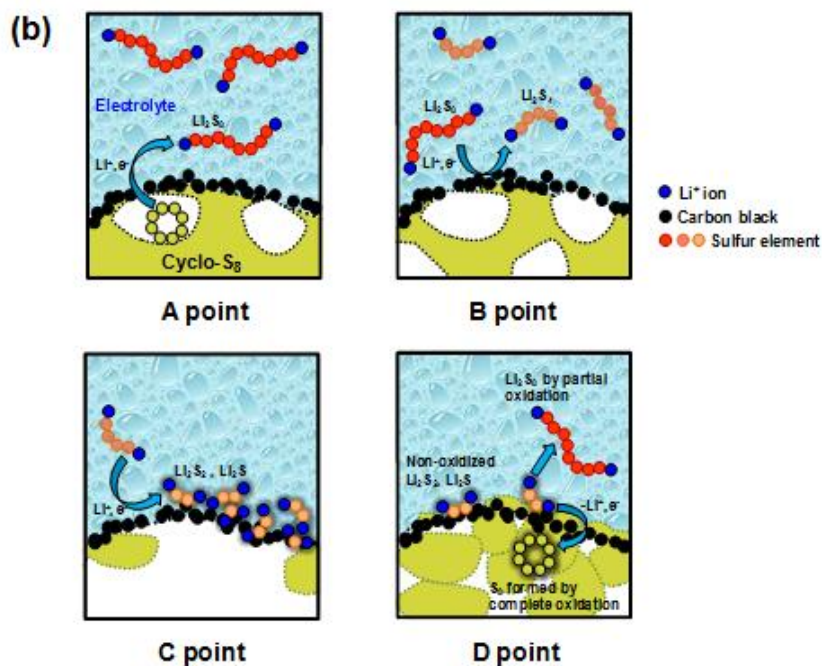
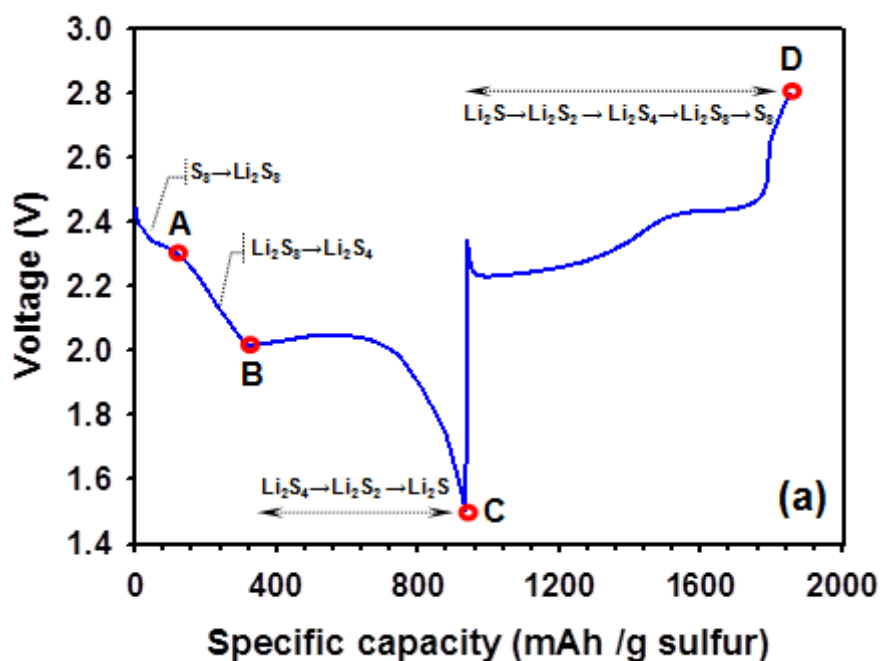


Figure 5. (a) First discharge and charge profiles of a Li-S cell between 1.5 and 2.8 V vs. Li/Li⁺ at a current density of 83.6 mA g⁻¹ (C/20). (b) Schematic drawing for a multistep phase transformation process of cyclo-S₈ to form various intermediate species (Li₂S_n, n=1~8).

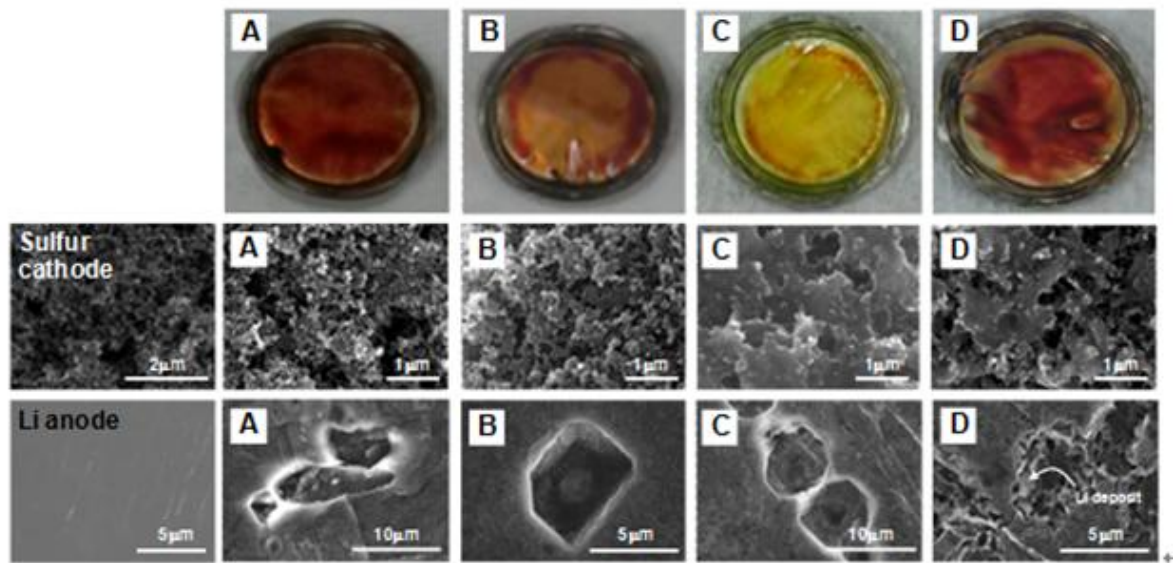


Figure 6. Photo of electrolyte solutions on the Li anodes at A, B, C, and D points (top). SEM images of the non-cycled sulfur cathode and the sulfur cathodes at A, B, C, and D points (middle). SEM images of the non-cycled Li anode and the Li anodes at A, B, C, and D points (bottom). All points are represented in Fig. 5(a).

3.2. Surface analysis of sulfur cathode at different depth of discharge and charge

To identify the solid products on the sulfur cathode at various discharged and charged states, the surface chemistry of the cathodes was investigated prior to conducting a DSC analysis. The C1s XPS spectra obtained from the cathodes at points A and B show three types of carbon (Figs. 7(a) and (b)): carbon black (284 eV), carbon bonded to hydrogen (CH₂-CF₂ (binder); 286 eV), and carbon bonded to fluorine (-CF₂- (binder); 290.8 eV).³⁷ The C1s XPS spectra of Fig. 7(c) clearly exhibit that the peak intensity assigned to the binder (CH₂-CF₂) at around 286 eV and 290.5 eV decreased after the cell was fully discharged to 1.5V, compared to Figs. 7(a) and (b). This is likely because solid products such as short-chain polysulfide species formed during the discharge process cover the cathode surface. In addition, a new peak, which can be assigned to Li-O-C- formed from reductive decomposition of the electrolyte during discharging, appeared at 288.7 eV.^{38,39,40} After the cell was fully charged up to 2.8V (Fig. 7(d)), the peak intensity at around 286 eV was much stronger than that of Fig. 7(a). This implies that the decomposition of the TEGDME solvent takes place and solid products containing the C-O-C group deposit on the cathode surface. After the full charging process, a very weak peak assigned to LiF at around 685 eV was observed, as shown in Fig. 7(d). This may be formed by reductive decomposition of LiTFSI salt (LiN(SO₂CF₃)₂ + ne⁻ + nLi⁺ → Li₃N + LiF + Li₂S₂O₄ + Li_xC₂F_y).^{37,41,42} This peak was not observed at the fully discharged state presumably due to a thick layer (insoluble short-chain polysulfide) covering the cathode surface, as shown at point C of Fig. 1(b). As clearly seen in the S2p XPS spectra of Fig. 7, the peaks from 160 eV to 164 eV (Li-S bond) gradually increased during the discharging process and then disappeared after the cell was fully charged to 2.8V. This indicates that solid products (Li₂S₂ or Li₂S) are formed during the discharge process and they are electrochemically oxidized to soluble polysulfide (not detected on the washed cathode surface) and sulfur during the charge process. In addition, peaks assigned to S-O₃ from oxidation of the polysulfide appeared at 167eV and 168.5eV during the first cycle and a peak attributed to -SO₂ from LiTFSI salt at 170eV was observed. Ex-situ XPS of the sulfur cathodes during the first cycle reveals that the electrochemical reduction of sulfur and the electrochemical oxidation of insoluble short-chain polysulfide intermediate species reversibly occur, and the polysulfide species can be oxidized by reacting with the electrolyte.

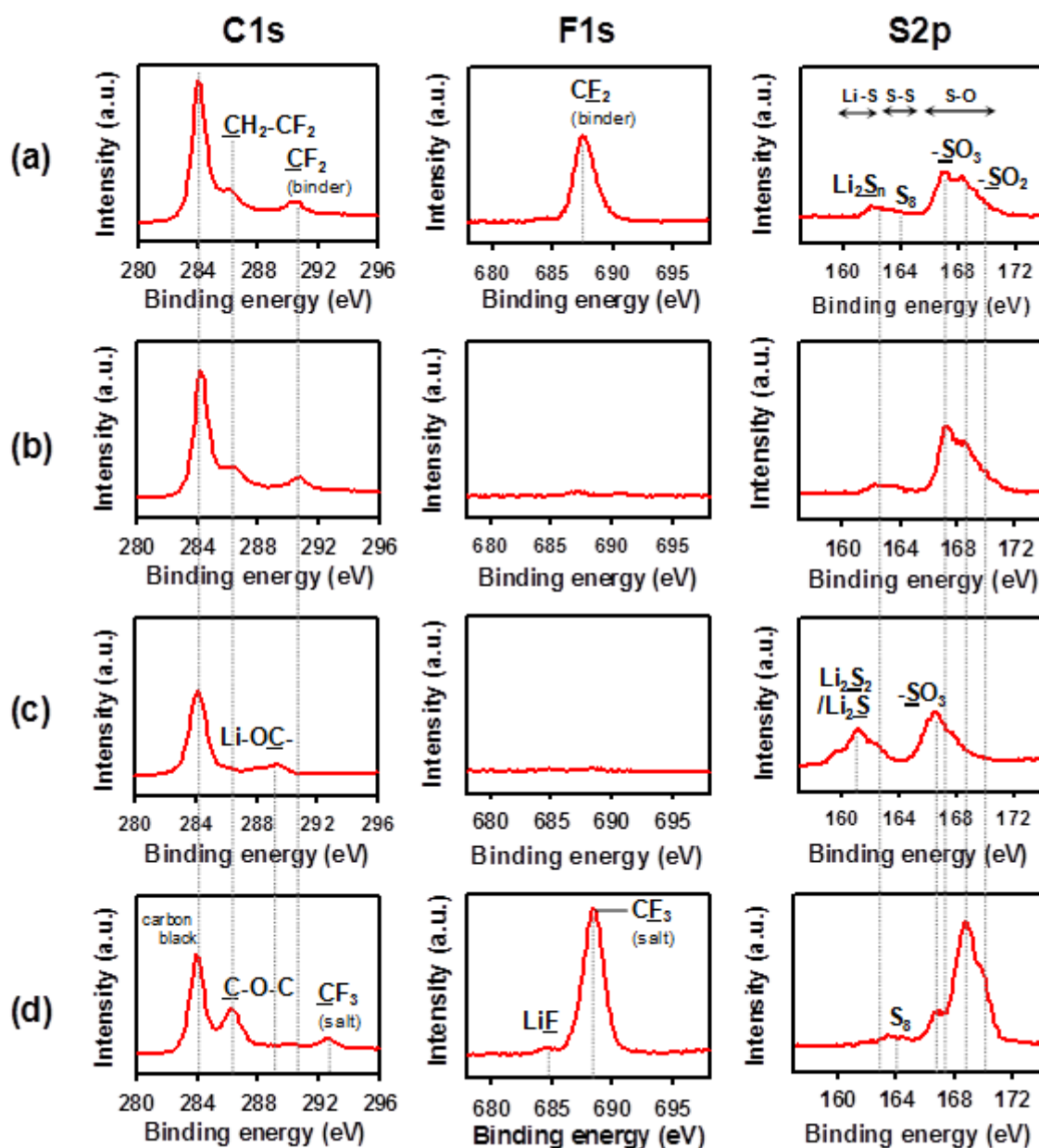


Figure 7. C1s, F1s, S2p XPS spectra of sulfur cathodes (a) discharged up to 2.3V, (b) discharged up to 2.02V, (c) fully discharged up to 1.5V, (d) fully charged up to 2.8V.

3.3. Thermal stability characteristics of sulfur cathode

Fig. 8 shows the DSC heating curves for the sulfur cathodes at various discharged and fully charged states. In addition, the DSC heating curves for TEGDME/1.3M LiTFSI electrolyte and for sulfur and Li_2S in the presence of an electrolyte are displayed at the bottom of Fig. 8. The cycled sulfur cathodes with the electrolyte were transferred into a hermetic DSC cell without a rinsing process. The very weak endothermic peak at 110 °C of Fig. 8(a) (A point) is ascribed to the melting of residual sulfur, which does not participate in electrochemical reduction to form soluble long-chain polysulfide species, because the elemental sulfur powder shows melting transition peaks at 110°C and 118°C. The sulfur cathodes discharged to points A and B of Fig. 1 exhibit a large exothermic peak at around 360 °C in the presence of an electrolyte. Note that sulfur and Li_2S with the electrolyte solution do not show an exothermic peak at around 360°C, as presented in Fig. 8. Therefore, the exothermic peak with a peak temperature of about 360°C is attributed to the thermal decomposition of long-chain polysulfide in the presence of the electrolyte, as depicted in Fig. 8(e). In the case of the fully discharged sulfur cathode with the electrolyte, the exothermic heat generation began at 170°C and very broad exothermic peaks were observed from 170°C to 300°C, as seen in Fig. 8(c). These exothermic peaks are analogous with peaks from thermal reactions of Li_2S with the electrolyte, as shown in the bottom of Fig. 8. Since Li_2S powder without an electrolyte does not produce any exothermic peak until 400 °C (Fig. 10(a)), broad exothermic peaks from 170 °C to 300 °C are attributed to thermal decomposition reactions between Li_2S and the electrolyte. Interestingly, the exothermic peak at about 360°C attributed to thermal decomposition between the electrolyte and long-chain polysulfide (Li_2S_n , $n=4-8$)-intermediate reaction species formed during the discharge process mostly disappeared in Fig. 8(c). These results suggest that when the cell is discharged to 1.5V, most of the long-chain polysulfide species are reduced to Li_2S_2 or Li_2S . Exothermic heat above 380 °C may originate from thermal decomposition of the electrolyte solution. Importantly, cycled sulfur cathodes exhibit no significant exothermic peaks from 200 °C to 300 °C except the broad exothermic peaks by the thermal reactions between $\text{Li}_2\text{S}_2/\text{Li}_2\text{S}$ and the electrolyte, as shown in Figs. 8(c) and (e). It should be noted that delithiated cathodes for Li-ion batteries deliver large exothermic heat at this temperature range.^{34,43} To compare the thermal stability of sulfur cathodes with that of lithium metal oxide-based cathodes, thermal properties of over-lithiated layered oxides (OLO), a cathode material that has recently received attention, were investigated in the presence of EC/EMC/DMC (3/4/3) with 1.3M LiPF_6 . Delithiated OLO charged up to 4.6V displays a very sharp and pronounced exothermic peak at 242°C in Fig. 8. The DSC results reveal that lithiated and delithiated sulfur cathodes with the electrolyte are thermally stable compared to lithium metal oxide-based cathodes. The fully charged sulfur cathode showed no broad exothermic peaks from 170 °C to 300 °C, which were observed at a

fully charged state, as shown in Fig. 8(d). This implies that the $\text{Li}_2\text{S}_2/\text{Li}_2\text{S}$ formed at point C mostly oxidized to elemental sulfur and polysulfide. Additionally, a small exothermic peak, which may be ascribed to the thermal reactions between long-chain polysulfide and the electrolyte (schematic representation for point D of Fig. 8(e)), appeared at around 360 °C. This peak is ascribed to residual long-chain polysulfide species (which did not undergo complete oxidation to elemental sulfur during the full charge process) that co-exist with elemental sulfur and thermally decompose.

To understand thermal runaway of Li-S batteries under harsh conditions, thermal properties of $\text{Li}_2\text{S}/\text{Li}$ and S/Li mixtures in the presence of an electrolyte were investigated, as shown in Figs. 9(a) and (d). The comparison of Figs. 9(a) and (b) clearly shows that the intensity of exothermic peaks for the $\text{Li}_2\text{S}/\text{Li}$ mixture with the electrolyte is greatly reduced above 330 °C. This is likely because Li_2S hinders the thermal reactions between the Li metal and the electrolyte at around 370°C. Importantly, the mixture of S and Li metal with the electrolyte presented a pronounced exothermic peak at 176°C after the sulfur melted, as seen in Figs. 9(d) and (g). This sharp exothermic peak is thought to be generated from thermal reactions between cyclooctasulfur and Li metal to form various polysulfide species (Li_2S_n , $n=1-8$). Although the mixture of S and Li metal contains no electrolyte, it showed a large exothermic peak, similar to the $\text{S}/\text{Li}/\text{electrolyte}$ mixture, as displayed in Figs. 9(d) and 10(d). This indicates that the noncycled Li-S cell can produce catastrophic exothermic heat at elevated temperatures. However, the $\text{Li}_2\text{S}/\text{Li}$ mixture as the fully discharged cell shows highly reduced exothermic peaks and an endothermic peak attributed to Li melting at 183 °C in the presence of an electrolyte (Fig. 9(a)). This means that fully discharged Li-S cells are more thermally stable than noncycled cells. The $\text{Li}_2\text{S}/\text{Li}$ mixture without an electrolyte generated exothermic heat at elevated temperatures of above 350 °C (Fig. 10(c)). It is surmised that this exothermic peak is produced by thermal reactions of Li_2S and Li metal, because Li_2S shows no exothermic peaks at elevated temperatures (Fig. 10(a)).

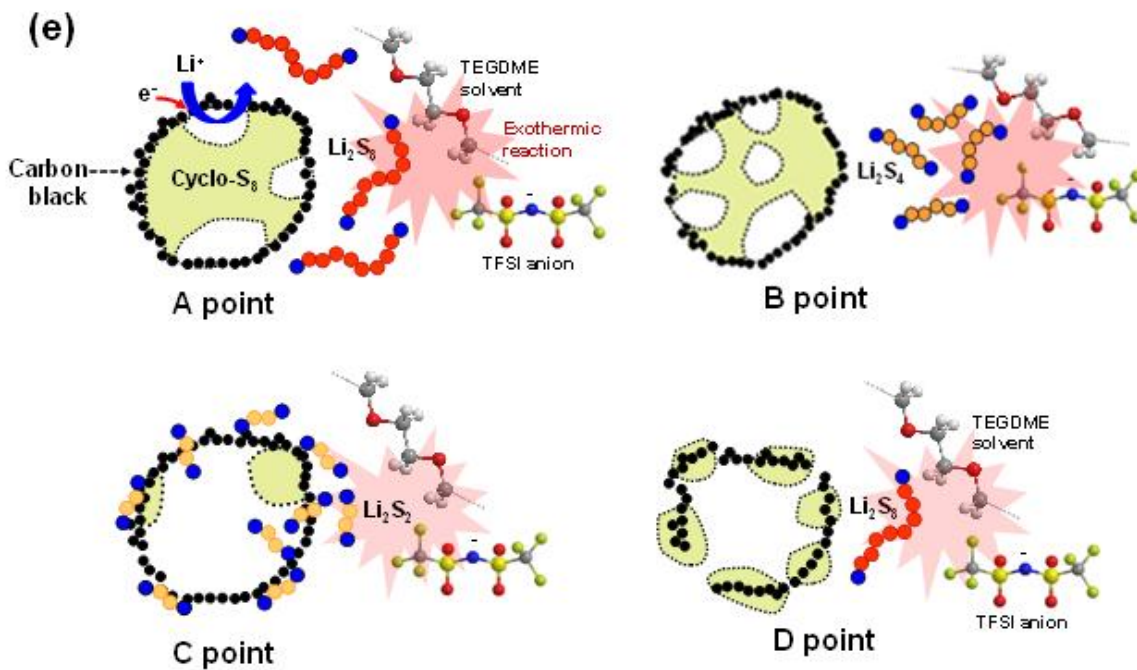
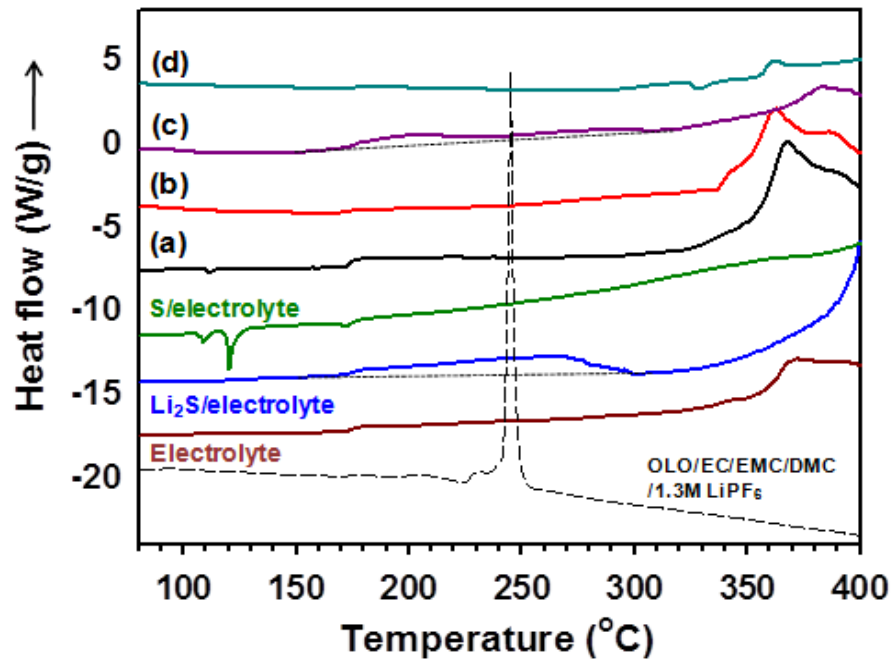


Figure 8. DSC heating curves of (a) sulfur cathode discharged to 2.3V, (b) sulfur cathode discharged to 2.02V, (c) sulfur cathode fully discharged to 1.5V, (d) sulfur cathode fully charged to 2.8V. All cathode samples for DSC measurements contain the electrolyte solution (1.3M LiTFSI in TEGDME). (e) Schematic for the thermal reactions of lithiated and delithiated sulfur cathodes in presence of TEGDME/1.3M LiTFSI. OLO represents over-lithiated layered oxides ($\text{Li}_x\text{Mn}_y\text{Co}_z\text{Ni}_a\text{O}_2$ cathode).

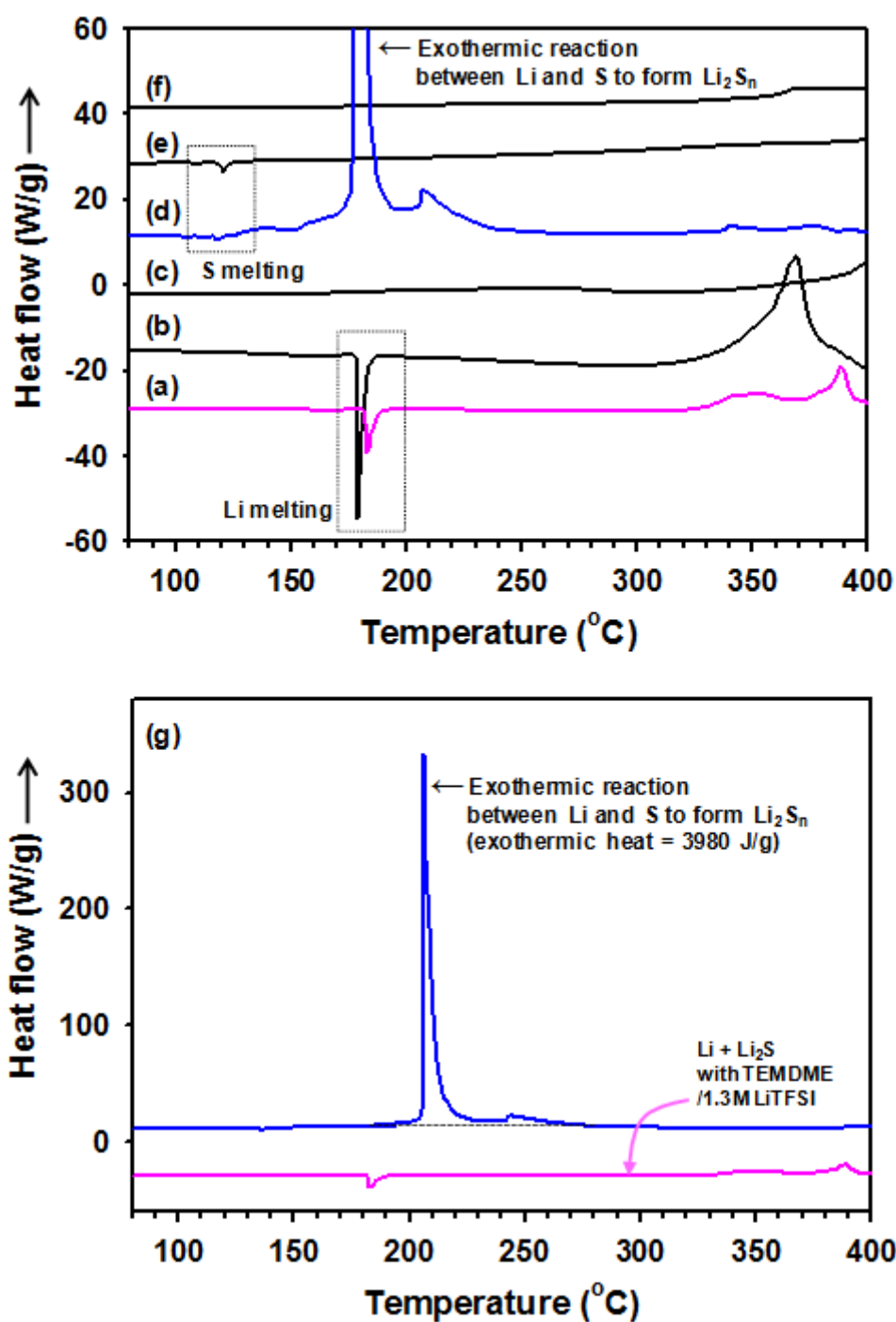


Figure 9. DSC heating curves of (a) Li₂S + Li metal with an electrolyte, (b) Li metal with an electrolyte, (c) Li₂S with an electrolyte, (d) S + Li metal with an electrolyte, (e) S with an electrolyte, (f) 1.3M LiTFSI in TEGDME electrolyte. (g) Comparison between S + Li metal with an electrolyte showing the exothermic peak at 176°C and Li₂S + Li metal with an electrolyte.

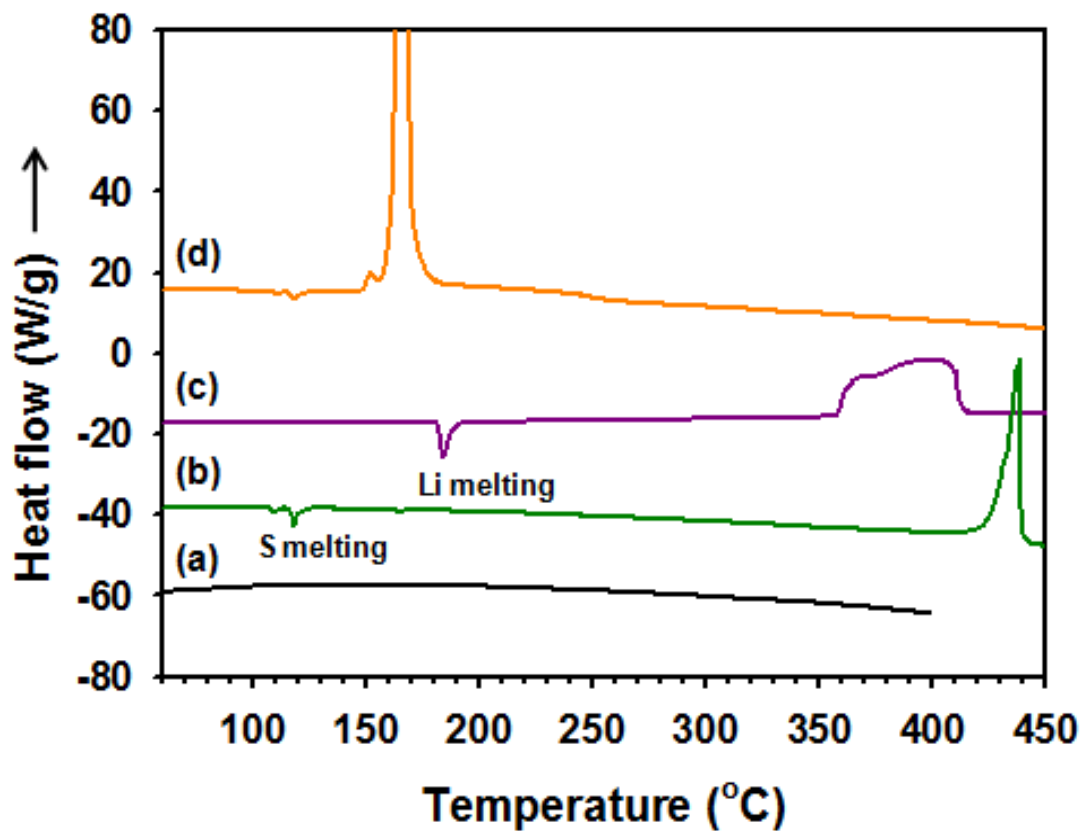


Figure 10. DSC heating curves of (a) Li_2S powder, (b) Sulfur powder, (c) Li_2S + Li metal, (d) S + Li metal in absence of an electrolyte.

4. Conclusions

The chemical structure of sulfur cathodes were clearly demonstrated by XPS analyses during the first discharge and charge processes. By using the DSC technique, we have shown that exothermic peaks for lithiated and delithiated sulfur cathodes in a Li-S battery are drastically reduced compared to a delithiated lithium metal oxide cathode in a Li-ion battery. The thermal reactions between Li metal and sulfur powder to form various lithium polysulfides generate catastrophic exothermic heat in the presence of the electrolyte, while the $\text{Li}_2\text{S}/\text{Li}/\text{electrolyte}$ mixture showed greatly reduced exothermic heat by thermal reactions.

CHAPTER III

The introduction of crosslinked gel polymer structure on a lithium anode for improving electrochemical performance of lithium sulfur batteries

1. Introduction

1.1. Li metal as an anode

Lithium has high energy density due to the lightest metal (equivalent weight = 6.94 g mol^{-1} , specific gravity = 0.53 g cm^{-3}) and also has high specific capacity (3860 mAh g^{-1}) as shown in Fig. 11.^{44,45} So this metal is very proper anode electrode lithium sulfur battery system. But, lithium as an anode electrode is very reactive material, which causes electrochemical reaction with polysulfides dissolved electrolyte, leading to form an unstable and non-uniform solid electrolyte interphase (SEI) layer. This response is more sustainable, function inside the cell is deteriorated such as fading specific capacity and cell explosion.^{23,26} Fig. 12 shows how to form of dendrite on the lithium.

1.2. Problems of lithium metal electrode

- Generation of dead lithium

During first charge, the deposited lithium is surrounded with the decomposed products and thus cannot participate in the discharge reaction.

- Consumption of active lithium

During 1st charge and discharge, both the deposited lithium and a part of lithium electrode is oxidized and thus the cavity in the surface of electrode is generated.

- Formation of dendritic lithium

Non-uniformity of the current distribution in the surface of lithium electrode makes the morphology of deposited lithium dendritic.

- Growth of SEI layer

The SEI layer continuously grows by the passivation of organic solvent and salt during repeated charge process.

Through these reactions, it can lead to various problems in lithium sulfur batteries. In lithium anode side: the non-uniform reaction of lithium surface, the risk of safety and increase of cell resistance of the battery due to the formation of a thick film of lithium dendrite. In sulfur cathode side: because of further reaction of between lithium and dissolved polysulfide, it is caused shuttle phenomenon (overcharge process) and alter structure of the lithium surface film.

The introduction of crosslinked gel polymer layer on lithium surface is expected to prevent further side reaction. Additionally, formation of dendritic layer can be suppressed during many cycling. This polymer type is crosslinked semi-IPN structure (semi-interpenetrating polymer network).^{6,23,26,27,46} Many researchers reported the structure of various kind of crosslinkers. They have ethylenically unsaturated groups such as allyl, acrylate or vinyl groups.^{47,48} Through thermal radiation by UV-curing, crosslinker is experienced polymerization (the part of chain is made up of a saturated hydrocarbon chain). It gives rise to improve the strength of the protective film. Also functional groups (oxygen bonds) in crosslinker are greater compatibility with electrolytes and then can reduced resistance of the cell. In addition, mobility of Li ion can be improved to pass through the protection layer.⁴⁹ Unlike typical polymer film, gel-polymer has sufficient liquid electrolyte. The space of crosslinked gel polymer can trap electrolyte, which is no side reaction with interfacial lithium/polymer film and it can also help mobility of Li cations during cycling. Generally, ionic conductivity of crosslinked gel polymer is around 10^{-3} S cm⁻¹ at 20 °C. In addition, the window of potential stability is good up to 4.5V vs. Li/Li⁺.⁴⁸ Therefore, it is possible to introduce to lithium anode surface as protective layer for improved lithium sulfur batteries properties. In this study, we demonstrated the effect of crosslinked gel polymer protection layer on the lithium anode and here the expected results as follows :

1.3. The role of the protection layer on lithium anode

- Morphology control of SEI layer.
- Suppressing dendrite formation
- Controlling decomposition products
- Blocking the reaction of lithium metal with polysulfides (Li₂S_n)
- Improved long cycling performance and coulombic efficiency.

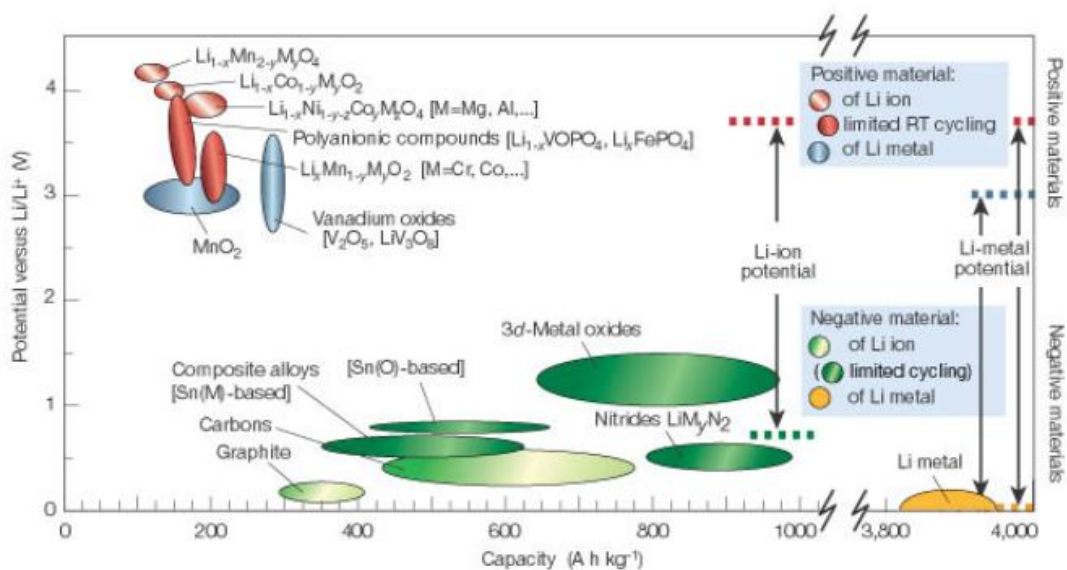


Figure 11. The graph of potential vs capacity of various cathode and anode materials.⁴⁵

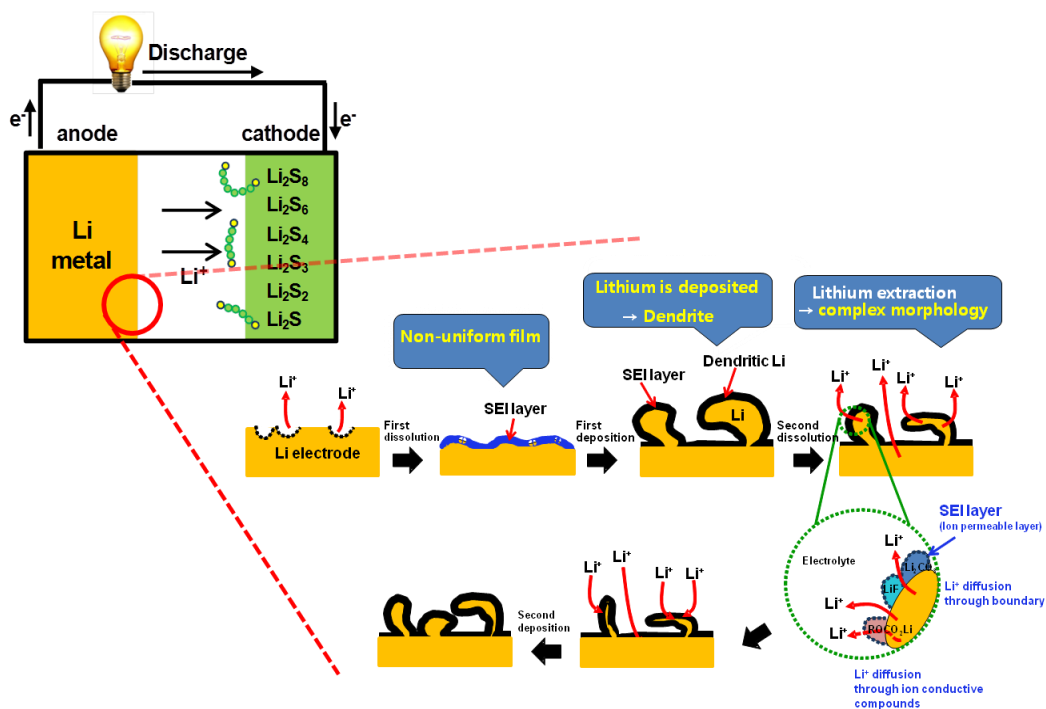


Figure 12. The non-uniform current distribution and high reactivity for lithium metal anode.

1.4. Researcher objectives

In this study, we introduce the protection layer of type for crosslinked gel polymer for lithium anode to prevent further reaction between lithium metal and polysulfide. Though Li symmetric cycling performance, FEC-based functional electrolyte in protection layer is good stability on interfacial lithium. After UV-curing polymerization, crosslinked gel polymer layer can effectively improve long cycling performance and coulombic efficiency during 100cycles at 0.1C rate. Depending on the cycle, the morphology change of lithium anode can be found. Protection layer can control of morphology of SEI and suppress dendrite formation during cycling.

2. Experimental

2.1. Preparation of semi-IPN gel-polymer matrix

Components are purified THF solvent (Aldrich), PVDF-co-HFP ($M_w=400,000$, Aldrich) linear polymer, photoinitiator (2-Hydroxy-2-methylpropiophenone, Aldrich), crosslinkers (1,4-butanediol diacrylate, trimethylolpropane ethoxylate triacrylate ($M_w = 428$), Aldrich), functional liquid electrolyte (1.3M LiTFSI / FEC, received from Soulbrain Co. Ltd.) as shown in Table 2. The mixture of linear polymer and THF solvent was stirred for 4 h at 60 °C. PVDF-co-HFP can act the role of thin film matrix and provide flexibility of protective film. And then, functional liquid electrolyte, crosslinkers and photoinitiator were added in mixed solution for 1 h at 25 °C. The well blended solution was fully coated on surface of lithium anode and dried for 10 min due to remove THF solvent. Go through this process, the matrix with liquid electrolyte trapped between spaces of polymer chain remained on lithium surface. After UV-curing in 2min, polymerization process, the type of semi-interpenetrating network (IPN) polymer structure was formed. This structure based on linear polymer and crosslinked polymer. Photoinitiator was added 0.6 wt% based on curable monomer. All process was procedure in glove box under vacuum condition. There shown the composition of protection layer as list of Table 3.

2.2. Lithium sulfur cell preparation and assembling

For the electrochemical tests, a mixture of 70 wt% elemental sulfur (100 mesh, Aldrich) and 20 wt% super P (as a carbon additive for conductivity enhancement, Timcal Inc.) was ball-milled, and then a 10 wt% poly(vinylidene fluoride) (PVDF) ($M_w = 534,000$, Aldrich) binder in anhydrous *N*-methyl-2-pyrrolidinone (NMP, Aldrich) was added to the mixture. After mixing the cathode slurry by using thinky mixer during 10min, it was cast on a piece of aluminum foil (20 μm) and then dried in a convection oven at 90 °C for 1 h. The thickness of all cathode films was about 29 μm and the sulfur loading was 0.7 mg cm^{-2} . As the count electrode, fresh Li metal foil (700 μm) used on the copper foil current correcter. Cell assembly was performed in glove box with 1.3M lithium bis(trifluoromethane sulfonyl)imide (LiTFSI) in tetra(ethylene glycol) dimethyl ether (TEGDME) (received from Soulbrain Co. Ltd.). Fig. 13 shows the schematic of internal lithium sulfur system.

2.3. Electrochemical cycling test

Galvanostatic discharge and charge cycling (WonATech WBCS 3000 battery measurement system) was performed in a potential window from 1.5 to 2.8 V vs. Li/Li^+ with a two-electrode 2032

coin-type cell. The sulfur cathode electrode functioned as the working electrode and the Li metal foil as the counter electrode. The first lithium insertion and extraction capacities were measured at a current density of 83.6 mA g^{-1} (C/20 rate) and long-life capacity were measured at a current density of 167.2 mA g^{-1} (C/10 rate) at $30 \text{ }^{\circ}\text{C}$. In addition, Li/Li symmetric cells were assembled 2016 coin cell. Cycling performance was measured at Li utilization 2% of 2.3 mAh and Li utilization 25% of 29 mAh (0.3C rate) at $30 \text{ }^{\circ}\text{C}$.

2.4. Electrochemical analysis

2.4.1. FE-SEM

The surface morphology of Li metal anodes was observed by means of a field emission scanning electron microscope (FE-SEM; JEOL JSM-6700F). During the acquisition of the SEM image, an energy dispersive spectrometer (EDS) mapping image was also used to determine the distribution of sulfur atom in the region under investigation. Li metal anodes retrieved from cells were put on a SEM holder in a glove box and the prepared samples were sealed with an aluminum pouch film under a vacuum. The samples were transferred from an aluminum pouch bag into a vacuum chamber for the SEM/EDS observation with exposure to atmosphere for 3 sec.

2.4.2. EIS and ATR-FTIR

To determine the resistance according to various amounts of functional electrolyte in protective layer, EIS (Electrochemical Impedance spectroscopy, HS Technologies) was used. Also, attenuated total reflectance-Fourier transform infrared (ATR-FTIR) spectra was recorded the presence of double bonds in crosslinkers at 1637 cm^{-1} and 812 cm^{-1} . The range of measured vibration frequency was from 4000 cm^{-1} to 650 cm^{-1} under a nitrogen atmosphere.

2.4.3. Refrigerated Bath Circulator

Ionic conductivity of crosslinked gel-polymer protection layer contained two types of crosslinkers was measured by Refrigerated Bath Circulator (made by DAIHAN Scientific Co., Ltd.) under the control of temperature from $0 \text{ }^{\circ}\text{C}$ up to $60 \text{ }^{\circ}\text{C}$. Dried polymer electrolyte in a rectangular frame for 2 h was prepared and samples were vacuum sealed with an aluminum pouch film in dry room.

Table 2. Chemical structure of linear polymer, crosslinkers, and photoinitiator for protection layer.

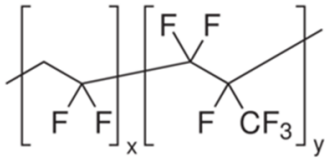
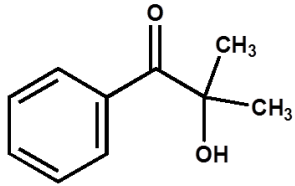
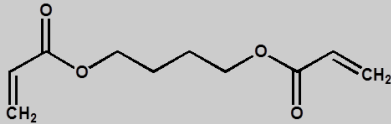
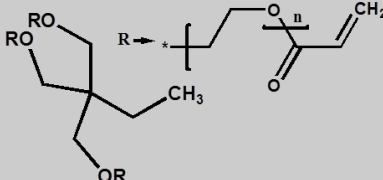
PVDF-co-HFP		2-Hydroxy-2-methylpropio phenone	
1,4-butandiol diacrylate (BDDA)		Trimethylol propane ethoxylate triacrylate (TMPETA 428)	

Table 3. Composition of protection layer.

	Crosslinking agent	^a PVDF-co-HFP	^b FEC 300%
	wt (%)		
Reference	-	-	-
Protection layer 1 ^c (BDDA)	16.66	16.66	69.68
Protection later 2 ^d (TMPETA 428)	16.66	16.66	69.68

^a PVDF-co-HFP is Poly(vinylidene fluoride-co-hexafluoropropylene). It is linear polymer.

^b FEC300% (1.3M LiTFSI/FEC, 300wt% based on curable monomer and linear polymer) is functional electrolyte in protection layer.

^c BDDA is 1,4 butanediol diacrylate and ^d TMPETA 428 ($M_w=428$) is trimethylolpropane ethoxylate triacrylate as curable monomer respectively.

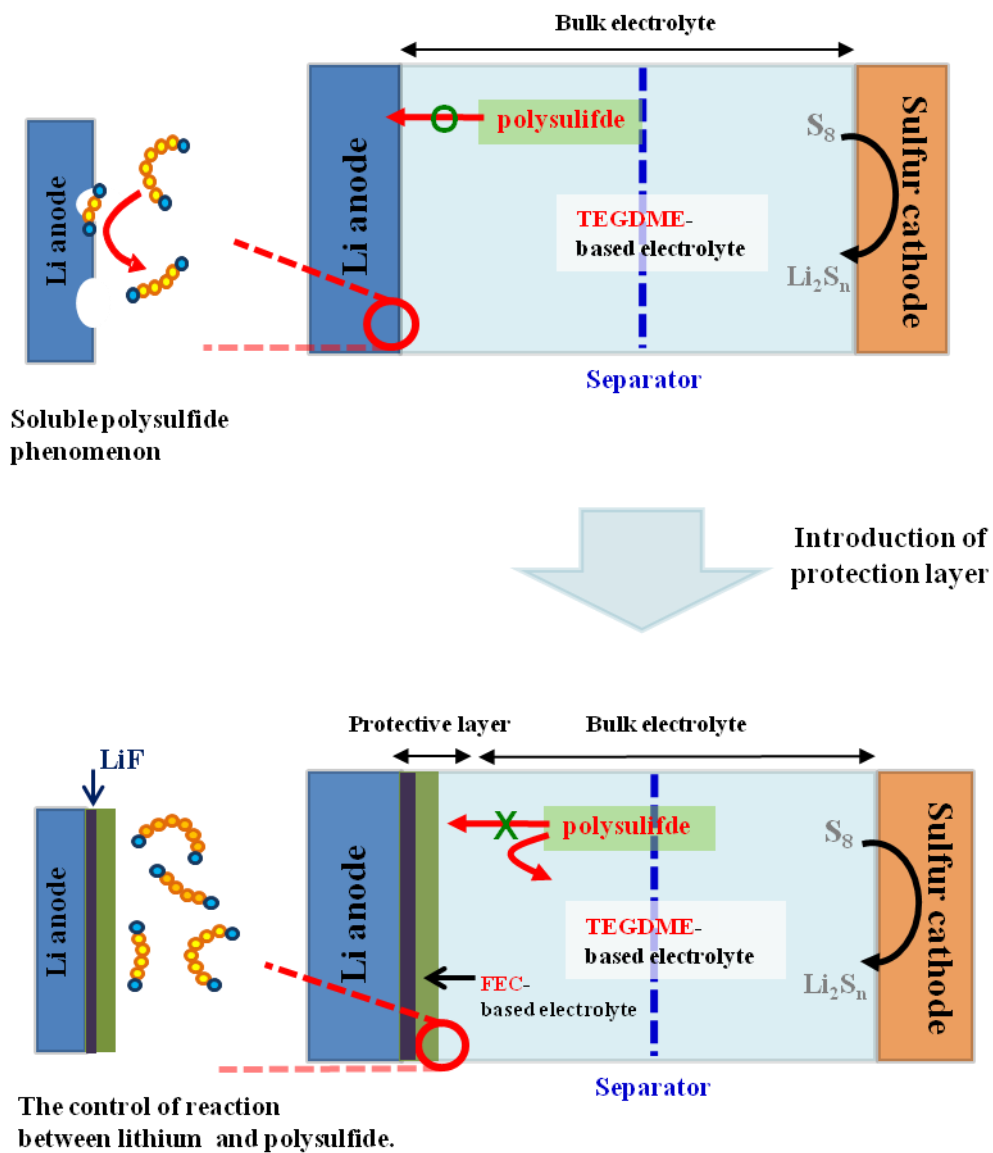


Figure 13. Schematic of internal lithium sulfur system of (a) non-protected lithium and (b) protected lithium anode.

3. Results and discussion.

3.1. Effect of fluoroethylene carbonate (FEC) based electrolyte on interfacial lithium anode

The positive effect of a fluoroethylene carbonate (FEC) based solvents is widely known to stabilize lithium anode surface.^{23,50,51} Fig. 14 presents the voltage profile of Li-Li symmetric cells with tetra(ethylene glycol) dimethyl ether (TEGDME) and fluoroethylene carbonate (FEC) based electrolytes. When using 100% FEC solvent, lithium stripping/deposition potential revealed good stability during cycling. The FEC, functional solvents in protection layer, can build-up of LiF-based SEI stabilizing the Li/electrolyte interface during repetitive charge and discharge. FEC is appropriate to the role of the functional electrolyte. The content of all FEC was based on weight (%) of curable monomer and linear polymer respectively. As clearly seen in Fig. 15(a), Li-S cell with 300% FEC-based electrolyte delivered the highest discharge capacity at precycle. This is likely because of low SEI resistance after precycle, as presented in Fig. 15(b). In addition, Fig. 15(c) revealed that the best long-cycle life was obtained for a Li-S cell with 300% FEC-based electrolyte. This indicates that 300% FEC-based electrolyte is more effective to prevent unwanted reaction between lithium surface and lithium polysulfide dissolved from the sulfur cathode during cycling. It is thought that the amount of 150% FEC-based electrolyte is not sufficient to ensure good Li ion mobility in a protective layer and to suppress the migration of polysulfide toward a Li anode. Eventually, a Li-S cell with 300% FEC-based electrolyte led to relatively low capacity and more significant overcharge behavior compared to other cells. Li-S cell with 400% FEC-based electrolyte increased the SEI resistance as well as C_t (charge transfer). This is probably because excess amount of the electrolyte in a protection layer does not maintain the mechanical stability of the protection layer when a Li anode contracts and expands during discharge and charge processes. From there results, we could confirm that the 300% FEC-based electrolyte is appropriate amount to prevent undesirable reaction between polysulfide and a Li anode, and form a stable SEI layer on the Li anode.

3.2. ATR-FTIR analysis of crosslinked polymer

The crosslinked gel polymer based on semi-IPN structure for protection layer on lithium anode is formed by UV-curing method. As can be seen in the SEM image as shown in Fig. 16, the crosslinked protective layer about 5.5 μm on surface of lithium anode can be successfully formed. To verify the cross-linking of the protective film, we analyzed by the FT-IR equipment. Figs. 17(a) and (b) shown the ATR-FTIR spectra of crosslinkers (BDDA, TMPETA 428), and after UV-curing in 2min as shown in Figs. 17(c) and (d). The peak formed at 1637 cm^{-1} and 812 cm^{-1} of all double bonds in monomers

disappeared by UV-curing.²⁶

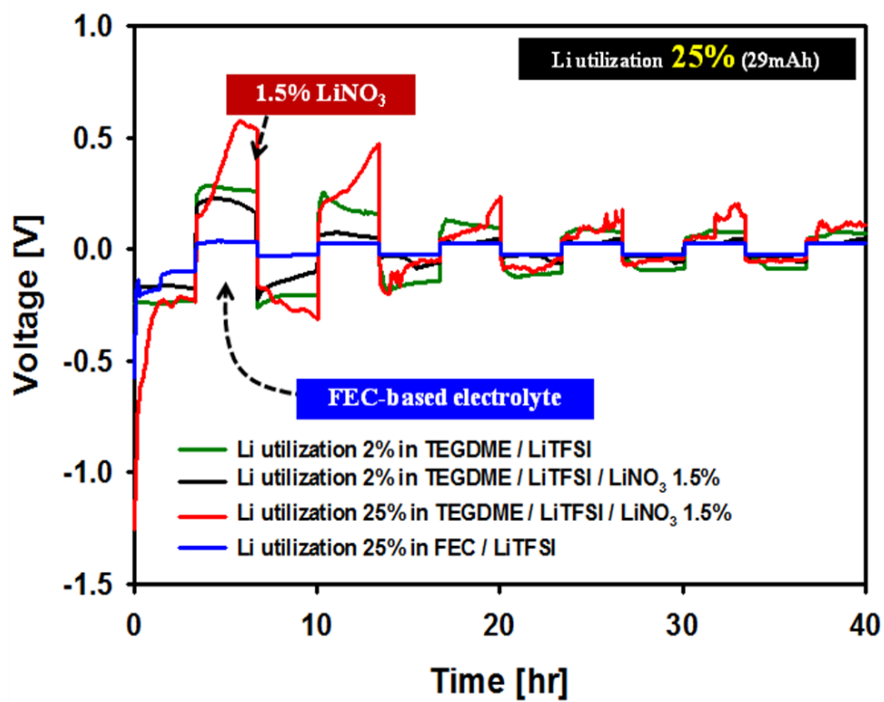


Figure 14. Galvanostatic cycling of Li symmetric cells with FEC- and TEGDME-based electrolytes.

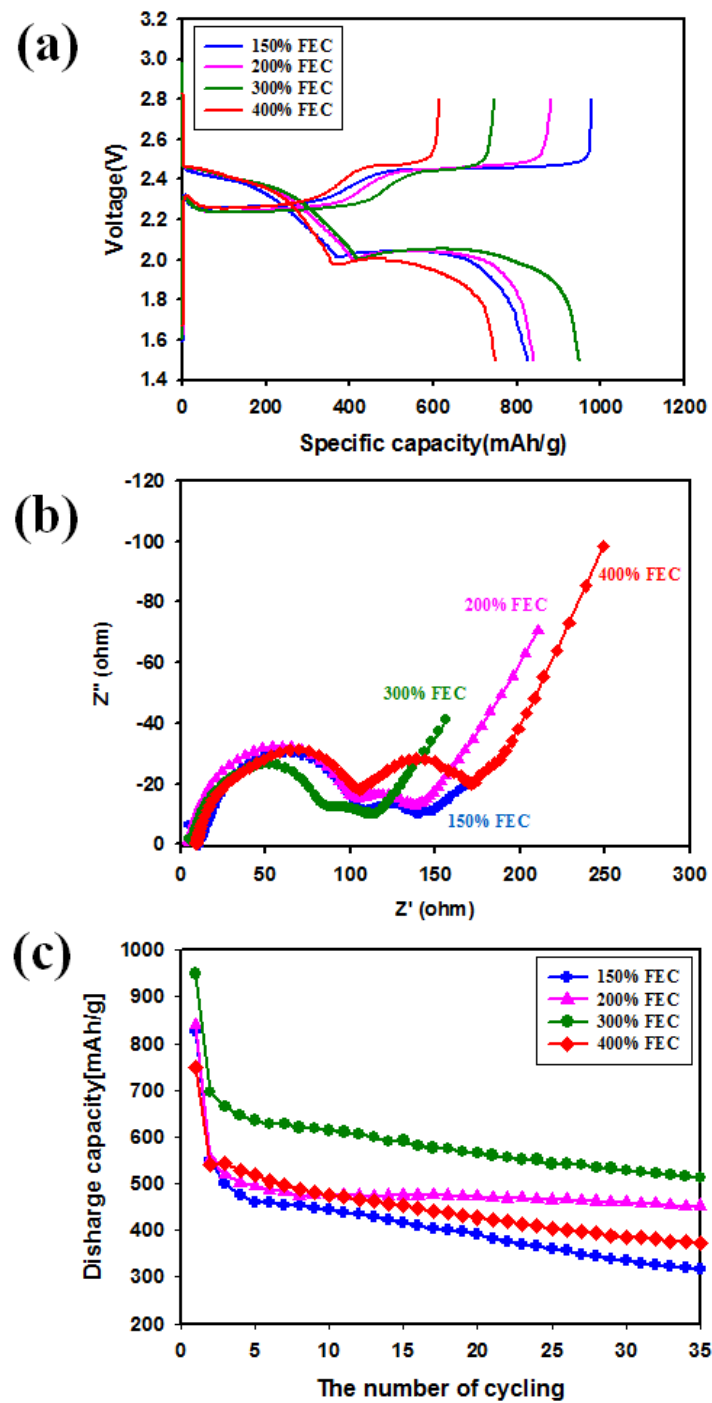


Figure 15. (a) Voltage profile of precycle at a rate of C/20. (b) EIS spectra of cells with various amounts of FEC-based electrolyte in a protection layer. (c) Cycling performance of Li-S cells with various amounts of FEC-based electrolyte in protection layer at a rate of C/10.

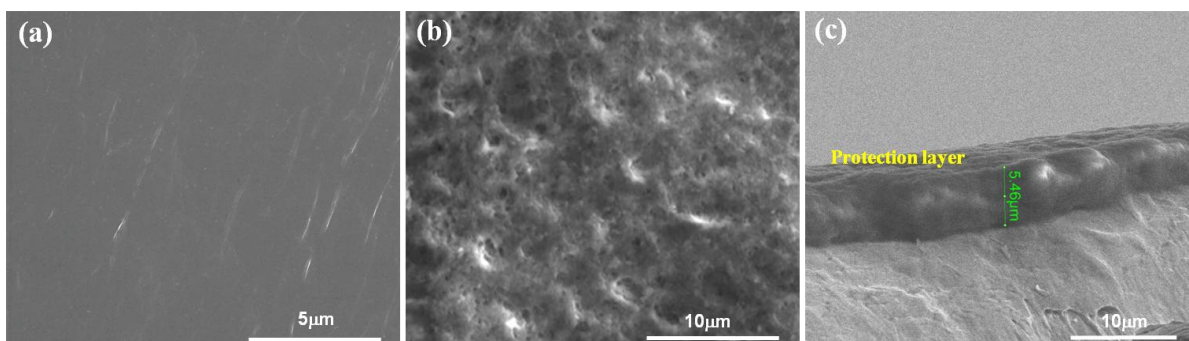


Figure 16. SEM images of (a) fresh lithium metal surface, (b) crosslinked protective layer and (c) image of cross-section about thickness of protective layer.

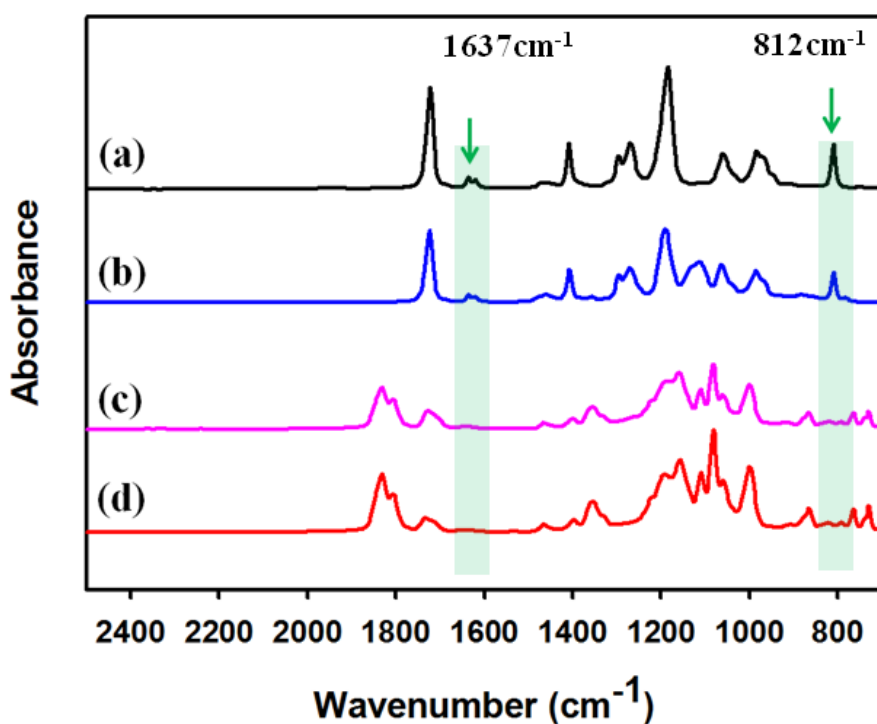


Figure 17. ATR-FTIR spectra for (a) BDDA, (b) TMPETA 428 crosslinkers. Spectra of crosslinked protection layer in present of (c) BDDA and (d) TMPETA 428 crosslinkers (after UV-curing).

3.3. Electrochemical properties in accordance with the crosslinkers in protection layer

The characteristic of long-life cycling performance of Li-S cells with and without a protective layer at 30 °C is shown in Figs. 18(a) and (b). In the case of Li anode without a protection layer, charge capacity was significantly increased by severe overcharging phenomena during 10cycles. On the other hand, the Li-S cells with a protection layer effectively inhibited overcharge behavior by the unwanted reaction between the Li anode and polysulfides and thereby showed greatly improved coulombic efficiency (> 80%). BDDA and TMPETA 428 used as a crosslinkers for the formation of the protection layer delivered similar discharge capacity and coulombic efficiency during 100cycles, as shown in Fig. 18. This implies that protection layers formed by these two crosslinkers effectively suppress the shuttle phenomena by polysulfide. Fig. 19 shows the SEM images of Li surface after cycles. Surface morphology of cycled Li anode was observed after removing a protection layer. Fig. 19(a) is the SEM image of fresh Li metal. Non-protected Li metal suffered from a severe overcharge reaction after precycle. However, protected Li anode was clean compared to non-protected Li anode. Only after 10cycles, the surface of non-protected Li anode was non-uniform and rough via significant reactions with the bulk electrolyte and polysulfides. On the contrary, it is clearly seen that the presence of the protection layer on the Li anode prevents unwanted reactions between a Li metal and polysulfides/electrolytes, and thereby makes Li anode surface more clean. Fig. 20 shows the surface morphology of protection layers on cycled Li anodes. After 100cycles, the protection layer was gradually damaged. However, they physically stayed on the Li anode during cycling, as presented in Fig. 20. According to many cycles, color of protection layer surface changed dark, as shown in Fig. 21. Fig. 22 presents the electrolyte color on a separator with the cycle number.³⁶ It seems that soluble lithium polysulfide dissolved from the sulfur cathode deposits on the protection layer without direct contact with the Li anode. Fig. 23 shows a photo of Li anode surface color after dismantling the cell. The region of removed polymer layer is bright colors, but protection layer is dark. Comparing to elemental S mapping results, distribution density of S is much higher. This indicates that protection layer effectively prevents the migration of polysulfides toward the Li anode during cycling.

3.4. The characteristic of C-rate according to protection layer

Fig. 24(a) shows the discharge capacity retention of Li-S cells with two different protection layers at various discharge rates at 30°C. The Li-S cell with the protective layer based on TMPETA 428 crosslinker exhibited relatively good rate capability. As shown in Fig. 18, the cycling performance behavior between BDDA and TMPETA 428 is similar at a low rate of C/10. However, TMPETA 428 can more swell when contacted with the bulk electrolyte due to presence of functional group with good compatibility with polar electrolyte components. Therefore, it is thought that ether functional groups of TMPETA 428 crosslinker make the migration of Li ions more easy at high C rates.⁴⁹ In addition, ionic conductivity of crosslinked polymer used TMPETA 428 is higher than that of BDDA-based protection layer, as shown in Fig. 25. Also, the Li-S cell with the protective layer based on TMPETA 428 presented much higher discharge capacity of 180 mAh g⁻¹ at a high rate of 3 C, compared to BDDA-based protection layer. The discharge capacity retention was analogous for two kinds of protection layers at low rates. Interestingly, discharge capacity rate and coulombic efficiency are increased together, as shown in Fig. 24(b). This indicates that high C rates can mitigate the movement of polysulfides dissolved from the sulfur cathode toward Li anode.

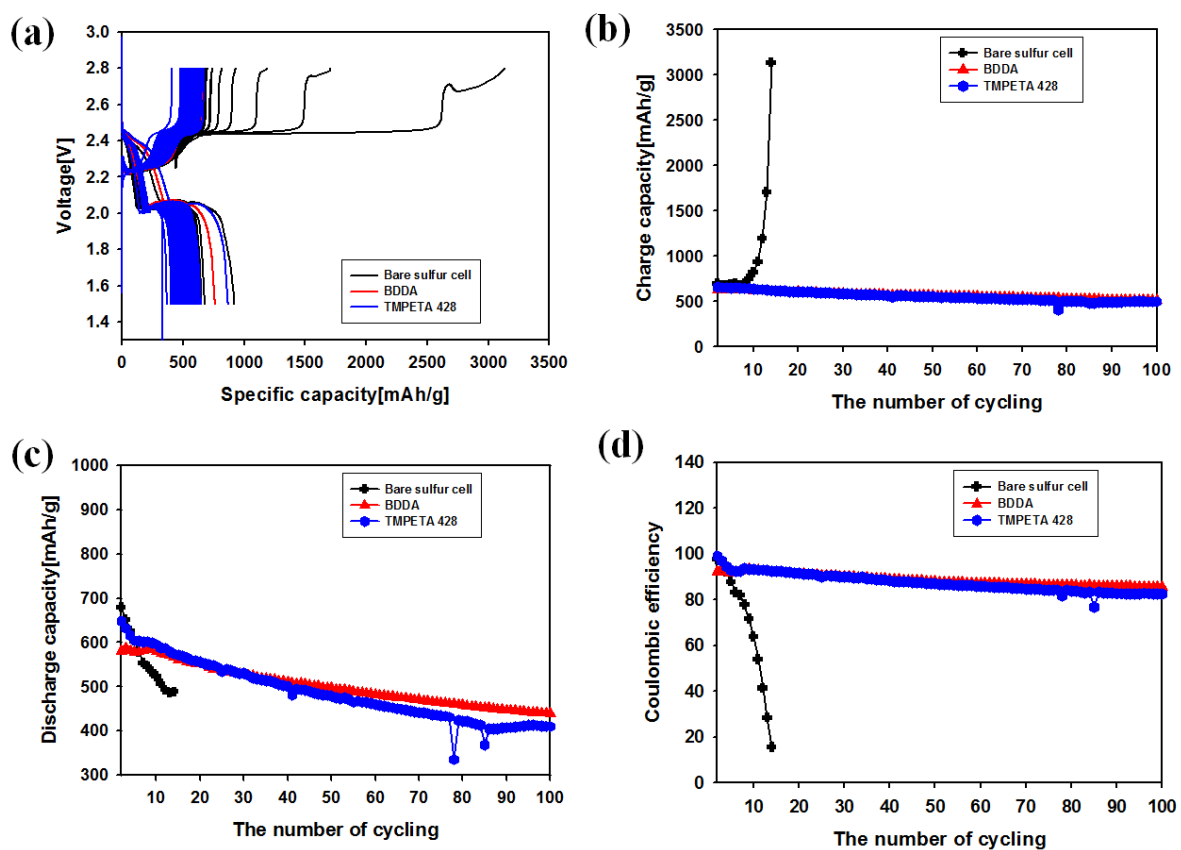
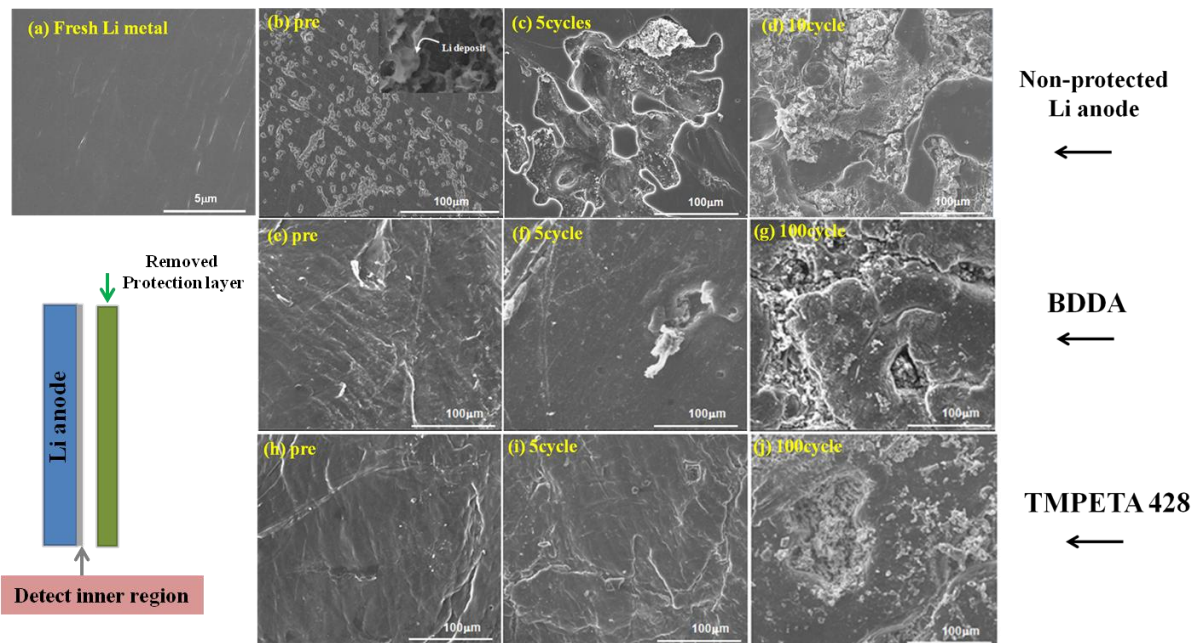


Figure 18. Cycling performance according to type of crosslinkers and in the presence of protection layer in lithium anode. (a) Voltage vs specific capacity profile, (b) charge capacity, (c) discharge capacity, (d) coulombic efficiency during 100cycles at a C/10 rate at 30 °C.



F

Figure 19. SEM images of lithium surface morphology. SEM images of (e) ~ (j) are lithium surface removed protection layer according to cycles.

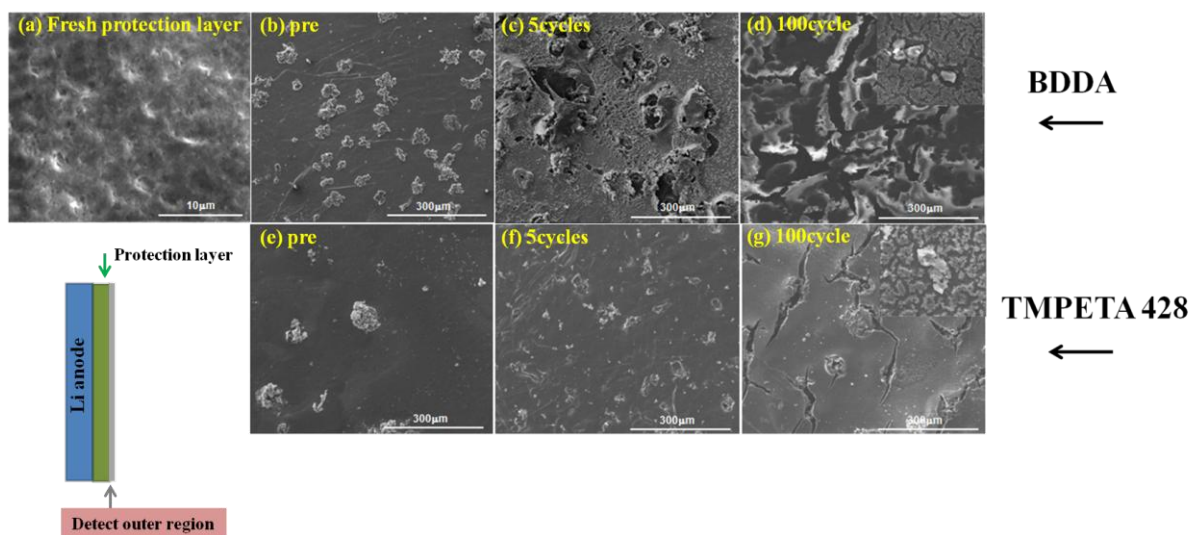


Figure 20. SEM images of lithium surface morphology. SEM images of (a) ~ (g) are morphology of protection layer on lithium surface according to cycles.

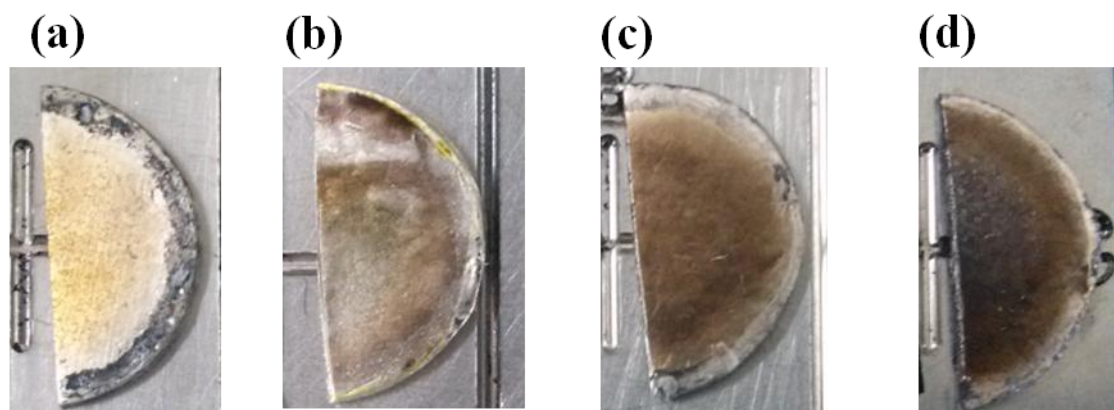


Figure 21. Change the color of the protection layer surface according to cycles. (a) precycle, (b) 5cycles, (c) 10cycles, (d) 30cycles.

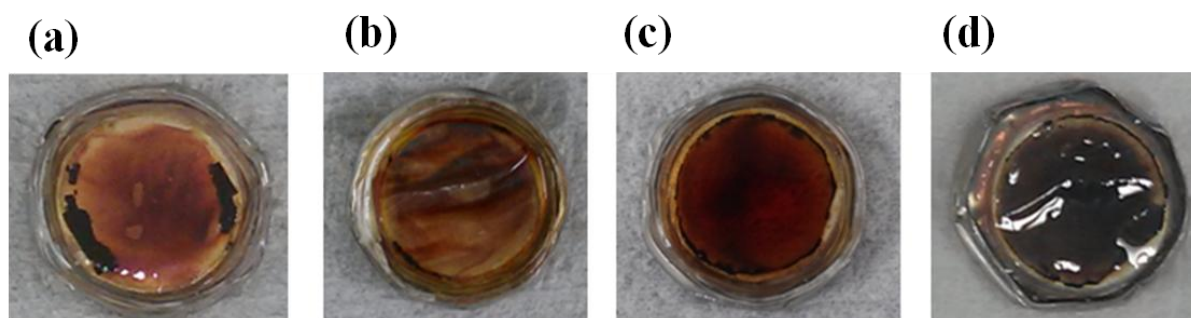


Figure 22. Change the color of the separator surface with the cycle number. (a) precycle, (b) 5cycles, (c) 10cycles, (d) 30cycles.

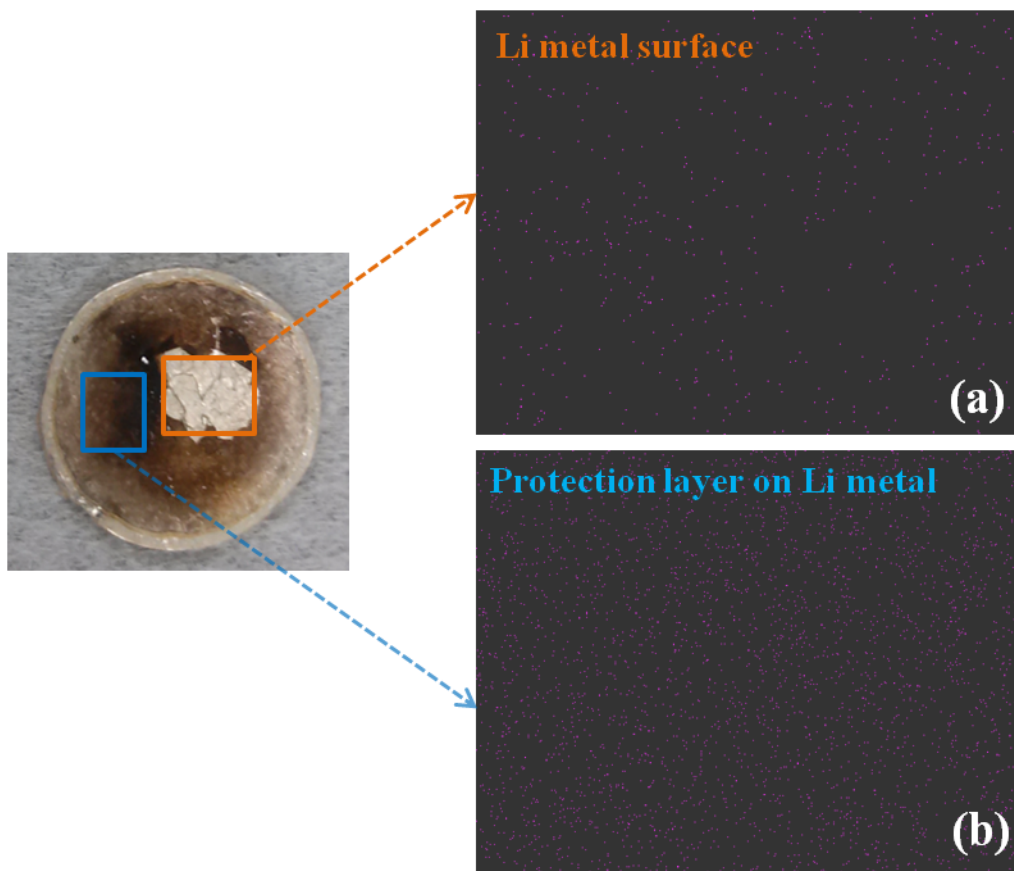


Figure 23. Comparison of the elemental S mapping images of (a) exposed lithium surface and of (b) protection layer surface after 10cycles.

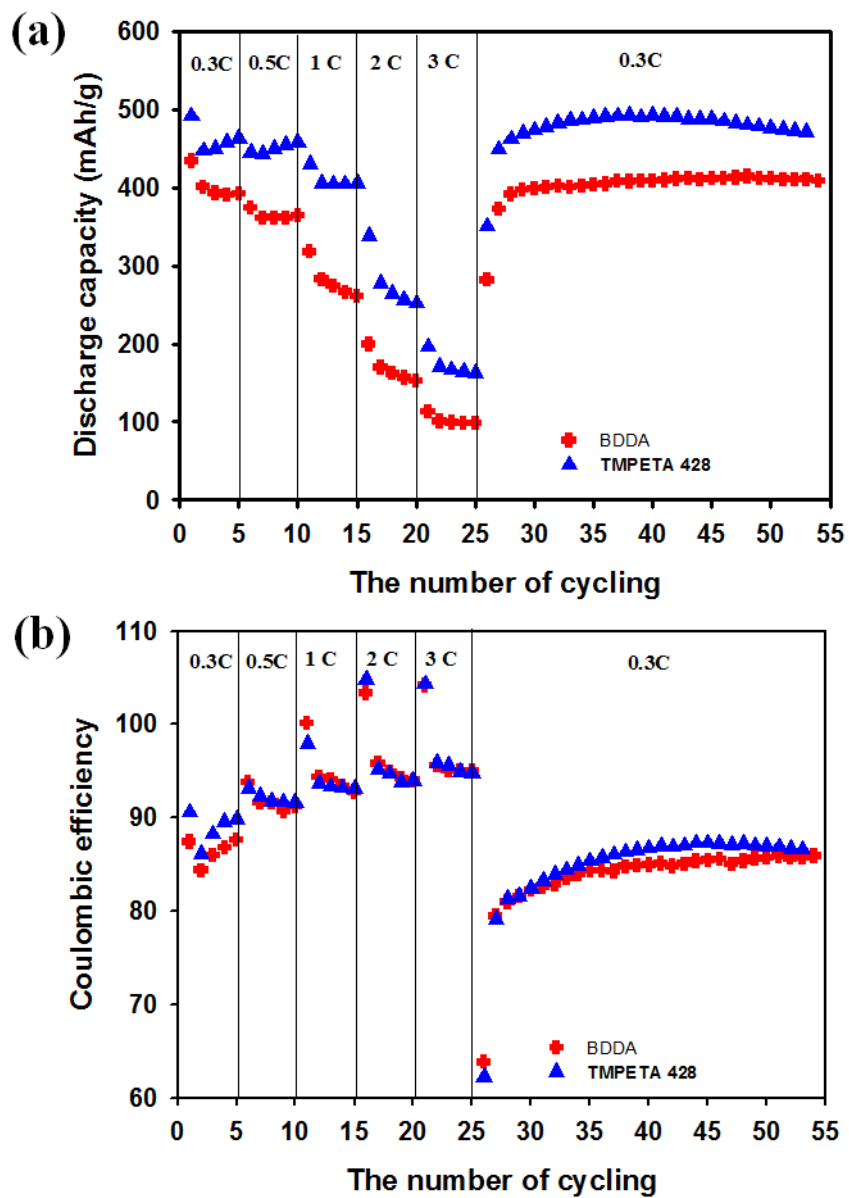


Figure 24. C-rate characteristics according to the kind of crosslinkers. (a) discharge capacity, (b) coulombic efficiency.

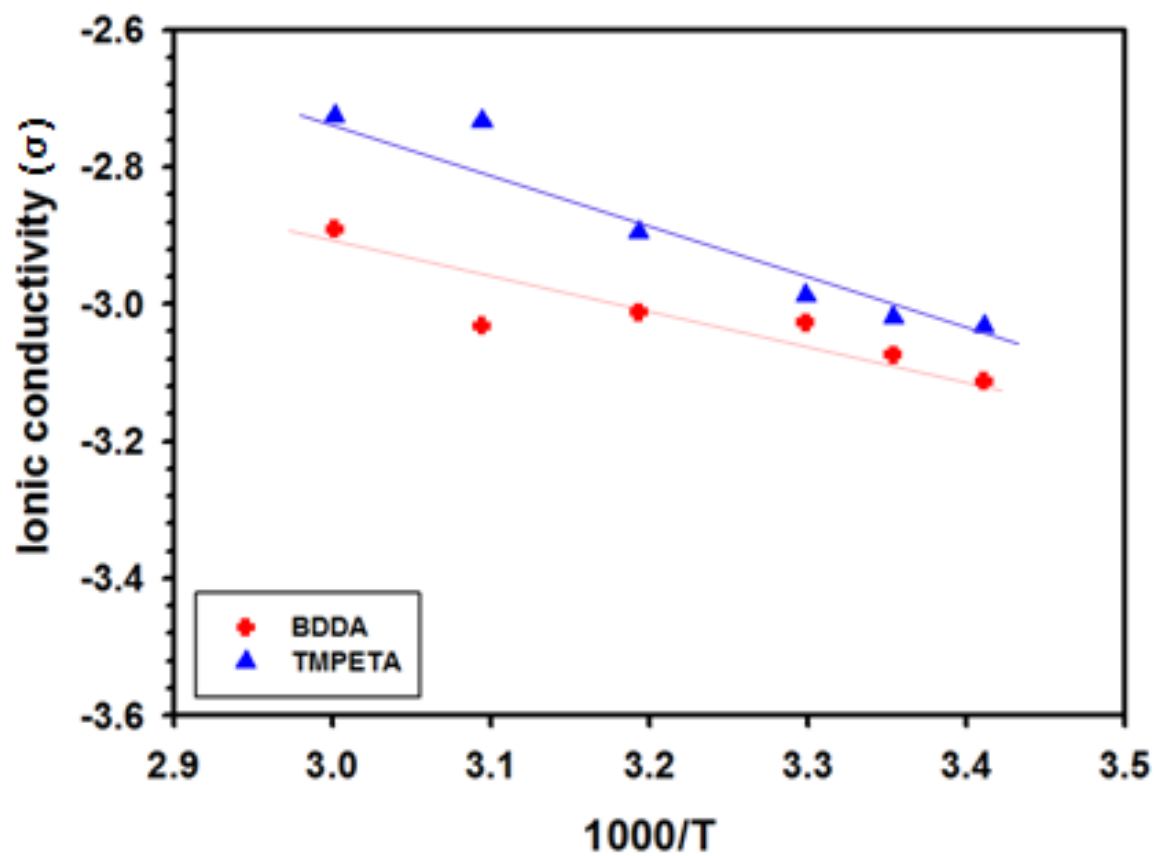


Figure 25. Comparison of the ionic conductivity of the crosslinked gel polymer according to the kind of the crosslinkers.

4. Conclusions

Li metal as anode electrode in lithium sulfur battery is very reactive material. During charge and discharge, dendritic lithium is formed by decomposition of electrolyte. Also the reaction between lithium metal and polysulfides causes overcharge process and capacity fading. We have confirmed the effect of protection layer coated lithium surface. Crosslinked gel polymer can prevent further reaction with polysulfide as well as creating a stable SEI layer on lithium anode. Gel-polymer can control of dendrite formation and morphology of lithium surface. Protection layer can be maintained after 100cycles, additionally, at a low and high-rate, long-life cycling performance shown good property compared to non-protected lithium.

References

1. Marmorstein, D.; Striebel, T. H. Y. K. A.; McLarnon, F. R.; Hou, J.; Cairns, E. J., Electrochemical performance of lithium/sulfur cells with three different polymer electrolytes. *Journal of Power Sources*.2000, 89, 219-226.
2. Thackeray, M. M.; Wolverton, C.; Isaacs, E. D., Electrical energy storage for transportation approaching the limits of, and going beyond, lithium-ion batteries. *Energy & Environmental Science*. 2012, 5, 7854-7863.
3. RAO, M. I. B., *U.S Patent Office*. 1968, No. 3,413,154.
4. Nole, D.; Moss, V., *U.S Patent Office*. 1970, No. 3,532,543.
5. Ji, X.; Nazar, L. F., Advances in Li-S batteries. *Journal of Materials Chemistry*.2010, 20, 9821-9826.
6. Lee, Y. M.; Choi, N.-S.; Park, J. H.; Park, J.-K., Electrochemical performance of lithium/sulfur batteries with protected Li anodes. *Journal of Power Sources*. 2003,119-121, 964-972.
7. R, J.; Akridge, Y. V.; Mikhaylik; White, N., Li/S fundamental chemistry and application to high-performance rechargeable batteries. *Solid State Ionics*.2004, 175, 243-245.
8. Bruce, P. G.; Freunberger, S. A.; Hardwick, L. J.; Tarascon, J.-M., Li-O₂ and Li-S batteries with high energy storage. *Nature materials*. 2012,11, 19-29.
9. V, Y.; Mikhaylik; Akridge, J. R., Low Temperature Performance of LiS Batteries. *Journal of The Electrochemical Society*. 2003, 150 (3), A306-A311.
10. Xu, K., Nonaqueous Liquid Electrolytes for Lithium-Based Rechargeable Batteries. *Chemical Reviews*. 2004, 104, 4303-4417.
11. Wang, L.; Zhang, T.; Yang, S.; Cheng, F.; Liang, J.; Chen, J., A quantum-chemical study on the discharge reaction mechanism of lithium-sulfur batteries. *Journal of Energy Chemistry*. 2013, 22, 72-77.

12. Jayaprakash, N.; Shen, J.; Moganty, S. S.; Corona, A.; Archer, L. A., Porous Hollow Carbon@Sulfur Composites for High-Power Lithium–Sulfur Batteries. *Angewandte Chemie-International Edition*.2011, *123*, 6026-6030.
13. Guo, J.; Xu, Y.; Wang, C., Sulfur-Impregnated Disordered Carbon Nanotubes Cathode for LithiumSulfur Batteries. *Nano Letters*. 2011, *11*, 4288-4294.
14. Aurbach, D.; Pollak, E.; Elazari, R.; Salitra, G.; Kelley, C. S.; Affinitob, J., On the Surface Chemical Aspects of Very High Energy Density, Rechargeable Li–Sulfur Batteries. *Journal of The Electrochemical Society*. 2009, *156* (8), A694-A702.
15. Xin, S.; Gu, L.; Zhao, N.-H.; Yin, Y.-X.; Zhou, L.-J.; Guo, Y.-G.; Wan, L.-J., Smaller Sulfur Molecules Promise Better Lithium-Sulfur Batteries. *Journal of the American Chemical Society*. 2012, *134*, 18510-18513.
16. Jung, Y.; Kim, S., New approaches to improve cycle life characteristics of lithium-sulfur cells. *Electrochemistry Communications*. 2007, *9*, 249-254.
17. Mikhaylik, Y. V.; Akridge, J. R., Polysulfide Shuttle Study in the Li/S Battery System. *Journal of The Electrochemical Society*.2004, *151*(11), 1969-1976.
18. Han, D.-H.; Kim, B.-S.; Choi, S.-J.; Jung, Y.; Kwak, J.; Parka, S.-M., Time-Resolved In Situ Spectroelectrochemical Study on Reduction of Sulfur in N,N'-Dimethylformamide. *Journal of The Electrochemical Society*. 2004, *151*(9), E283-E290.
19. Wang, C.; Chen, J.-j.; Shi, Y.-n.; Zheng, M.-s.; Dong, Q.-f., Preparation and performance of a core-shell carbon/sulfur material for lithium/sulfur battery. *Electrochimica Acta*. 2010, *55*, 7010-7015.
20. Barchasz, C. I.; Molton, F.; Duboc, C.; Leprêtre, J.-C.; Patoux, S. b.; Alloin, F., Lithium/Sulfur Cell Discharge Mechanism: An Original Approach for Intermediate Species Identification. *Analytical Chemistry*. 2012, *84*, 3973-3980.
21. Yuan, L. X.; Feng, J. K.; Ai, X. P.; Cao, Y. L.; Chen, S. L.; Yang, H. X., Improved dischargeability and reversibility of sulfur cathode in a novel ionic liquid electrolyte. *Electrochemistry Communications*. 2006, *8*, 610-614.

22. Liang, C.; Dudney, N. J.; Howe, J. Y., Hierarchically Structured Sulfur/Carbon Nanocomposite Material for High-Energy Lithium Battery. *Chemistry of Materials*. 2009, 21, 4724-4730.
23. Song, J.-H.; Yeon, J.-T.; Jang, J.-Y.; Han, J.-G.; Lee, S.-M.; Choi, N.-S., Effect of Fluoroethylene Carbonate on Electrochemical Performances of Lithium Electrodes and Lithium-Sulfur Batteries. *Journal of The Electrochemical Society*. 2013, 160(6), A873-A881.
24. Yeon, J.-T.; Jang, J.-Y.; Han, J.-G.; Cho, J.; Lee, K. T.; Choi, N.-S., Raman Spectroscopic and X-ray Diffraction Studies of Sulfur Composite Electrodes during Discharge and Charge. *Journal of The Electrochemical Society*. 2012, 159(8), A1308-A1314.
25. He, X.; Pu, W.; Ren, J.; Wang, L.; Wang, J.; Jiang, C.; Wan, C., Charge/discharge characteristics of sulfur composite cathode materials in rechargeable lithium batteries. *Electrochimica Acta*. 2007, 52, 7372-7376.
26. Cho, N.-S.; Lee, Y. M.; Park, J. H.; Park, J.-K., Interfacial enhancement between lithium electrode and polymer electrolytes. *Journal of Power Sources*. 2003, 119-121, 610-616.
27. Choi, N.-S.; Lee, Y. M.; Cho, K. Y.; Ko, D.-H.; Park, J.-K., Protective layer with oligo(ethylene glycol) borate anion receptor for lithium metal electrode stabilization. *Electrochemistry Communications*. 2004, 6, 1238-1242.
28. Aurbach, D.; Pollak, E.; Elazari, R.; Salitra, G.; Kelley, C. S.; Affinitob, J., On the Surface Chemical Aspects of Very High Energy Density, Rechargeable Li-sulfur batteries. *Journal of The Electrochemical Society*. 2009, 156(8), A694-A702.
29. Liang, X.; Wen, Z.; Liu, Y.; Wu, M.; Jin, J.; Zhang, H.; Wu, X., Improved cycling performances of lithium sulfur batteries with LiNO₃-modified electrolyte. *Journal of Power Sources*. 2011, 196, 9839-9843.
30. Zhang, S. S., Effect of Discharge Cutoff Voltage on Reversibility of Lithium/Sulfur Batteries with LiNO₃-Contained Electrolyte. *Journal of The Electrochemical Society*. 2012, 159(7), A920-A923.
31. Choi, N. S.; Chen, Z. H.; Freunberger, S. A.; Ji, X. L.; Sun, Y. K.; Amine, K.; Yushin, G.; Nazar, L. F.; Cho, J.; Bruce, P. G., Challenges Facing Lithium Batteries and Electrical Double-Layer Capacitors.

Angewandte Chemie-International Edition. 2012, 51 (40), 9994-10024.

32. Shim, J.; Striebel, K. A.; Cairns, E. J., The lithium/sulfur rechargeable cell - Effects of electrode composition and solvent on cell performance. *Journal of the Electrochemical Society*. 2002, 149 (10), A1321-A1325.

33. Barghamadi, M.; Kapoor, A.; Wen, C., A Review on Li-S Batteries as a High Efficiency Rechargeable Lithium Battery. *Journal of the Electrochemical Society*. 2013, 160 (8), A1256-A1263.

34. Lee, K. S.; Myung, S. T.; Kim, D. W.; Sun, Y. K., AlF₃-coated LiCoO₂ and Li[Ni_{1/3}Co_{1/3}Mn_{1/3}]O₂ blend composite cathode for lithium ion batteries. *Journal of Power Sources*. 2011, 196 (16), 6974-6977.

35. Han, S. C.; Song, M. S.; Lee, H.; Kim, H. S.; Ahn, H. J.; Lee, J. Y., Effect of multiwalled carbon nanotubes on electrochemical properties of lithium sulfur rechargeable batteries. *Journal of the Electrochemical Society*. 2003, 150 (7), A889-A893.

36. Li, Y. J.; Zhan, H.; Liu, S. Q.; Huang, K. L.; Zhou, Y. H., Electrochemical properties of the soluble reduction products in rechargeable Li/S battery. *Journal of Power Sources* 2010, 195 (9), 2945-2949.

37. Diao, Y.; Xie, K.; Xiong, S. Z.; Hong, X. B., Insights into Li-S Battery Cathode Capacity Fading Mechanisms: Irreversible Oxidation of Active Mass during Cycling. *Journal of the Electrochemical Society*. 2012, 159 (11), A1816-A1821.

38. Schechter, A.; Aurbach, D.; Cohen, H., X-ray photoelectron spectroscopy study of surface films formed on Li electrodes freshly prepared in alkyl carbonate solutions. *Langmuir*. 1999, 15 (9), 3334-3342.

39. Ota, H.; Sakata, Y.; Wang, X. M.; Sasahara, J.; Yasukawa, E., Characterization of lithium electrode in lithium imides/ethylene carbonate and cyclic ether electrolytes II. Surface chemistry. *Journal of the Electrochemical Society*. 2004, 151 (3), A437-A446.

40. Enslin, D.; Thissen, A.; Jaegermann, W., On the formation of lithium oxides and carbonates on Li metal electrodes in comparison to LiCoO₂ surface phases investigated by photoelectron spectroscopy. *Applied Surface Science* .2008, 255 (5), 2517-2523.

41. Aurbach, D.; Chusid, O., The use of in situ Fourier-transform infrared spectroscopy for the study of surface phenomena on electrodes in selected lithium battery electrolyte solutions. *Journal of Power Sources*. 1997, 68 (2), 463-470.
42. Balbuena, P. B.; Wang, Y., *Lithium-Ion Batteries: Solid-Electrolyte Interface*. Imperial College Press ed.; 2004.
43. Cho, J., Correlation between AlPO_4 nanoparticle coating thickness on LiCoO_2 cathode and thermal stability. *Electrochimica Acta* 2003, 48 (19), 2807-2811.
44. Ota, H.; Sakata, Y.; Otake, Y.; Shima, K.; Ue, M.; Yamaki, J., Structural and functional analysis of surface film on Li anode in vinylene carbonate-containing electrolyte. *Journal of the Electrochemical Society*. 2004, 151 (11), A1778-A1788.
45. Tarascon, J. M.; Armand, M., Issues and challenges facing rechargeable lithium batteries. *Nature* 2001, 414 (6861), 359-367.
46. Lee, Y. M.; Choi, N. S.; Park, J. H.; Park, J. K., Electrochemical performance of lithium/sulfur batteries with protected Li anodes. *Journal of Power Sources*. 2003, 119, 964-972.
47. Safranski, D. L.; Gall, K., Effect of chemical structure and crosslinking density on the thermo-mechanical properties and toughness of (meth)acrylate shape memory polymer networks. *Polymer* 2008, 49 (20), 4446-4455.
48. Kim, S. I.; Kim, H. S.; Na, S. H.; Moon, S. I.; Kim, Y. J.; Jo, N. J., Electrochemical characteristics of TMPTA- and TMPETA-based gel polymer electrolyte. *Electrochimica Acta* 2004, 50 (2-3), 317-321.
49. Karadag, E.; Saraydin, D., Swelling studies of super water retainer acrylamide/crotonic acid hydrogels crosslinked by trimethylolpropane triacrylate and 1,4-butanediol dimethacrylate. *Polymer Bulletin*. 2002, 48 (3), 299-307.
50. Mogi, R.; Inaba, M.; Jeong, S.-K.; Iriyama, Y.; Abe, T.; Ogumia, Z., Effects of Some Organic Additives on Lithium Deposition in Propylene Carbonate. *Journal of the Electrochemical Society*. 2002, A1578-A1583.
51. Choi, N.-S.; Yew, K. H.; Lee, K. Y.; Sung, M.; Kim, H.; Kim, S.-S., Effect of fluoroethylene

carbonate additive on interfacial properties of silicon thin-film electrode. *Journal of Power Sources*. 2006, 1254-1259.

